Tuning the Viscoelastic Properties of Hyaluronic Acid-Based Thiolene Hydrogels for Tissue Engineering Applications

By Philip M Elrod

Submitted to the graduate degree program in Bioengineering and the Graduate Faculty of the University of Kansas in partial fulfillment of the requirements for the degree of Master of Science.

Committee members

X

Dr. Jennifer L. Robinson
Committee Chair

X

Dr. Alan M. Allgeier

X

Dr. Stevin H. Gehrke

Date Defended: April 22, 2022

The thesis committee for Philip Matthew Elrod certified that

this is the approved version of the following thesis:

Tuning the Viscoelastic Properties of Hyaluronic Acid-Based Thiolene Hydrogels for Tissue Engineering Applications

X

Chair: Jennifer L. Robinson

Date Approved: June 13, 2022

Abstract

Osteoarthritis (OA) affects 300 million people worldwide, with roughly 80% of these cases being knee OA. While there are many events that promote OA, injury and maladaptive repair of the meniscal discs is a major factor. Considerable prior research has examined mechanisms behind regenerating avascular meniscal tissue, however, many limitations in both *in vivo* and *in vitro* models exist. The literature demonstrates that hyaluronic acid (HA) has viscoelastic properties conducive to tissue regeneration and specifically the rate of stress relaxation creates a regenerative cellular response not yet examined in meniscal cells[1]. The linear HA polymer has limited mechanical properties; however, functionalization using adaptive chemical moieties to promote crosslinking has been previously used to optimize those properties for tissue engineering applications. Common examples include use as injectables and scaffolds which creates further potential for implementation as extracellular matrix (ECM) mimics for *in vitro* studies of cell behavior and differentiation.

HA functionalized with increasing amounts of pentenoic acid (PHA) provided a thiol-ene "click" chemistry platform to promote chain growth polymerization, and optimize crosslink density to modulate hydrogel network properties, including swelling and compressive properties. Herein, the role of degree of -ene substitution, modulated by the HA monomer to pentenoic acid molar ratio, on crosslink density and resulting network properties was investigated in water, phosphate buffered saline, and human cell complete growth media. Crosslink density was shown modulate the mechanical and physical characteristics of the hydrogels including swelling, compression, viscoelasticity, uniform network formation and degradation. The increased crosslinking led to reduction in swelling, increase in compressive modulus, a shift in the viscoelastic properties and reduction in mesh size and rate of degradation. In PBS and complete growth media with increased

ionic strength, osmotic deswelling resulted in reduced swelling and reduced compressive modulus values of the gels.

PHA hydrogels showed considerable progress toward the goal of producing a tunable hydrogel that resembles the ECM physically and viscoelastically. The robust production delivered reproducible degree of substitution (DoS) as a function of input ratios. The limitations of the system were apparent as the DoS increased and the possible occurrence of intramolecular thiol-ene reactions were increasing. By performing experiments in ionic solutions to mimic physical conditions it was evident that the ionic contributions from the solutions decreased the range of outputs for the gels due to osmotic deswelling. Even with osmotic deswelling the system is robust and allows for the control of the viscoelastic components of these hydrogels. This control is fundamental for utilization of the PHA system in future stress-relaxation studies. Across all conditions, the viscoelastic properties followed trends shown in native soft tissues including meniscal tissue, which is of interest for future studies.

Acknowledgements

I would like to thank Dr. Robinson for her willingness to take on a very non-traditional graduate student and to patiently work with me through the process as I redeveloped and reshaped myself as an engineer after so many years as a biochemist. Her instruction and system of cooperation have helped me to recreate myself into a mindset for this new Bioengineering thread.

I would like to thank my committee members. Dr. Gehrke for all the time and effort helping bring me to a better understand polymer chemistry and its vast expanse of use in BioE. Also, Dr. Allgeier for sharing his knowledge in the best uses of analytical technologies and opening my mind to the use of these technologies in ways that I hadn't imagined possible.

I would like to thank all of the members of the Robinson lab who have spent time working through experiments and data analysis with me so I can update and get on board with the fast-moving current of technology and software. Kayla Castillo for working so diligently and talking through the research and papers even when she was busy with class. Elizabeth Aikman for holding out hope when it seemed that logic and science were failing. Kevin Chavez, Kelsey Knewtson, Katherine Meinhold, Pamela Johnson, John Bradford, Nathan Ohl, Justin Lehtinen, Alyssa Morrell, Kylie Burkey, and Jacob Hodge for making all the long days in the lab more fun and manageable. A special thank you to Murilo Toledo Suekuni for all his efforts in running the LF NMR data and spending so much time helping me to understand this technique and the value of the data.

I would like to thank many other graduate and undergraduates that put up with my seemingly difficulty time adjusting and encouraged me to keep plugging away. This includes Morgan Riley, Sarah Woolfolk, Sarah Freeburne, Emily Freeburne, Matthew Jaeschke, and Kyle Boone.

A special thanks to Pat and Sam who had to listen to me complain about having to do homework again and helped me figure out how to be a old dude working with a younger generation on their terms. Thanks for letting me vent and see how there is still a lot of fun to be had.

Lastly, I would like to thank my best friend, Kelly!!! It seems like we have made it through more of these than most people ever see in a lifetime. I know it sucks to watch me procrastinate and hate writing, but thanks for sticking with me even when I shut down and just pretend the world doesn't exist. Maybe this one will be the last one.?!

Table of Contents

List of Tables

List of Figures

List of Equations

Equation 1 $$q = \frac{m_s}{m_d}$$

Equation 2 $$\varepsilon = \frac{(L_o - L)}{L_o}$$

Equation 3 $$E = \frac{\sigma}{\varepsilon}$$

Equation 4 $$\rho_x = \frac{G}{RT\, V_2{}^{1/3} V_{2r}{}^{2/3}}$$

Equation 5 $$G = 1/3E$$

Equation 6 $$V_2 = 1/q$$

Equation 7 $$\varepsilon = \theta K_\varepsilon$$

Equation 8 $$\sigma = FK_\sigma$$

Equation 9 $$K_\sigma = \frac{G_c}{A}$$

Equation 10 $$E' = cos\delta(\frac{\sigma}{\varepsilon})$$

Equation 11 $$E" = sin\delta(\frac{\sigma}{\varepsilon})$$

Equation 12 $$tan\delta = \frac{E"}{E'}$$

Equation 13 $$Monomers\ (M1) = Da(\frac{1.66*10^{-24} g}{Da})(\frac{mol\ HA}{379.32\ g})(\frac{6.022*10^{23}\ molecules}{mol\ HA})$$

Equation 14 $$M1\ x\ desired\ DoS = required\ DoS\ (RM)$$

Equation 15 $$RM = (M1\ x\ hPHA\ DoS)(wt\%high) + (M1\ x\ lPHA\ DoS)(wt\%low)$$

Introduction

Around 250-300 million people worldwide are affected by osteoarthritis (OA)[2-5] . Of these cases, around 80% are varying levels of knee OA[6, 7]. Knee OA is a systemic inflammatory disease that diminishes and destroys healthy articular cartilage through persistently elevated levels of pro-inflammatory cytokines and a reduction in the ability to produce the key extracellular matrix (ECM) molecules[4, 7]. Meniscal tears are the most prevalent intra-articular knee injury and pose significant risk in the development of OA. The disease state is exacerbated by the fact that the cartilage and fibrocartilage of the knee contains avascular regions that lack sufficient nutrients for repair, coupled with low mitotic activity, thus exhibiting extremely limited ability to self-heal[7-9]. Risk factors for knee OA include age, gender, obesity, and trauma[2, 4, 8]. The prevalence of OA increases with age and women are considerably more likely to suffer from knee OA as age increases [6]. Current treatments include pharmaceuticals[7], microfracture[9] , stem cell therapy[10], surgical implantation of scaffolds [8] and utilizing injectable hydrogels[11]. Current tissue engineering approaches using hydrogels to repair and regenerate the meniscus do mimic the native ECM to a degree but are still limited[1, 12]. Considerable work has been done to understand cell differentiation in the meniscus required for new ECM production, organization, and regeneration of the tissue[13], the importance of viscoelastic ECM properties for meniscal repair and regeneration[14] and how hydrogels are pivotal in the translation of regenerative strategies from *in vitro* to *in vivo*[1, 5] but there is still a long way to go to move away from treatment to a cure.

Meniscus and ECM

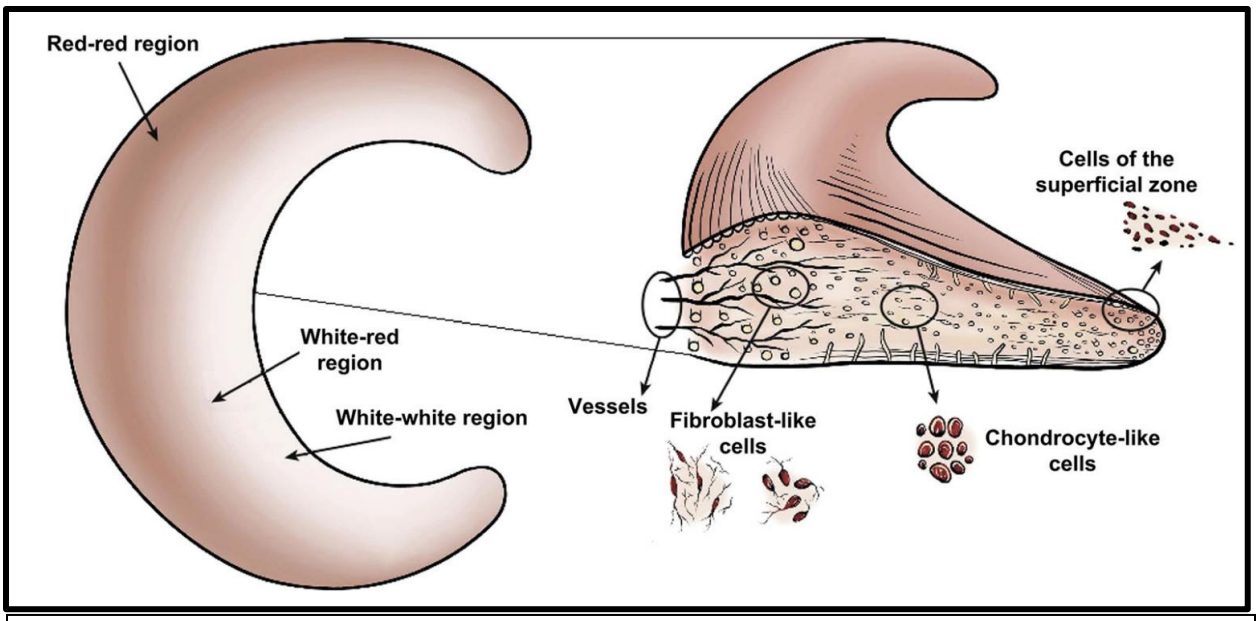

Figure 1. Knee Meniscus. The left frame shows the 3 regions of the meniscus; red-red, red-white and white-white. The right frame shows the transition from fibroblast to chondrocytes moving from red to white zone. It also shows that the red is vascularized and the white is avascular. (Reproduced from Bochynska)[15]

The meniscus of the knee, Figure 1, is in appearance a simple set of two "C" shaped (semi-lunar), wedge shaped disc that function to provide stability to the knee, joint congruency, distribute force, enact homeostasis for the articular cartilage and provide lubrication[15-18]. The meniscus is divided into 3 regions; the red-red, the red-white and the white-white. The outer, red-red region, is vascularized and contains fibroblast-like fibrochondrocytes. The middle, red-white region, is minimally vascularized and transitions away from fibroblast-like to chondrocyte-like fibrochondrocytes. The inner, white-white region, is primarily composed of chondrocyte-like fibrochondrocytes [15, 19]. The remainder of the meniscus is made up of the ECM, predominantly composed of collagen type I, in the outer, vascularized zone and collagen type II in the inner, avascular zone[15] . The positioning and alignment of the cells and the ECM components allows for the meniscus to repeatedly distribute the forces primarily from the femur[17], Figure 2. Highly aligned collagen fibers follow the curvature of the meniscus and are coordinated with the radial

bundles of collagen that are interwoven with the circumferentially distributed bundles. The circumferentially aligned fibers take on stresses when the meniscus is compressed through the vertical axis, reducing hoop stresses[17], and the shear forces are distributed along the radial collagen fibers, reducing displacement[20]. The structure and function of the meniscus and the ECM are highly complex and still being elucidated, but there is much to learn about the forces that inform tissue regeneration through mechanotransduction and gene regulation.

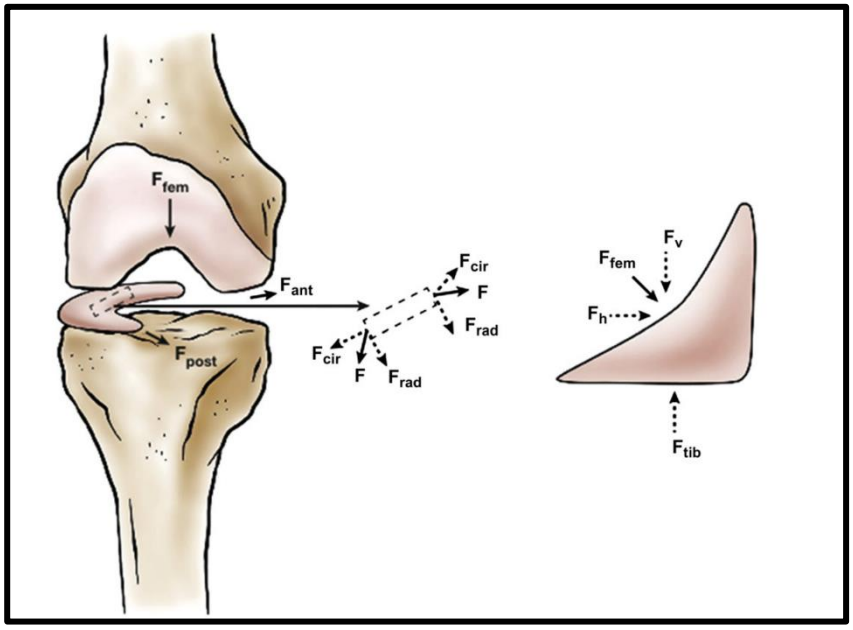

Figure 2. Free body diagram of the forces exerted on the knee and resulting forces exerted by the meniscus. (Reproduced from Markis)[17]

Hyaluronic Acid

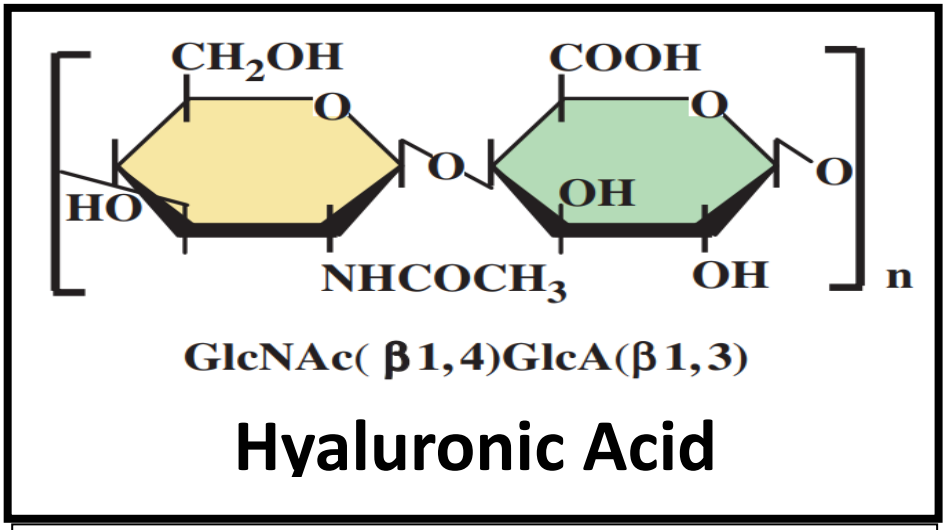

Figure 3. Chemical Structure of Hyaluronic Acid. (Reproduced from Itano)[28]

Hyaluronic acid (HA), Figure 3, is an unbranched, non-sulfated glycosaminoglycan (GAG) that is a component of the ECM[21] and is composed of repeat units of (1-3)-β-N-acetyl-D-glucosamine and (1-4)-β-glucuronic acid[22, 23]. Overall, HA has a negative charge distribution which results in the hydrogel having an equilibrium water constant > 90%[24, 25]. This allows HA to hold up to 1000x its polymer weight in water, thus showing similar physical characteristics to soft tissue[22, 26]. HA in native physiological conditions can range in size from 100 kDa – 8000 kDa[23]. The molecular weight and concentration of HA can affect its biophysical and mechanical properties. Low MW HA has been shown to contribute to pro-inflammatory response, promoting cell attachment[24], pro -angiogenesis, stimulation of gene expression in some epithelial cells[22], release of heat shock protein and a non-apoptotic cellular response[27]. Whereas high MW HA shows anti-angiogensis[28], immunosuppression, anti-inflammatory response[24] inhibition of cell proliferation[24], cell quiescence[22] and increased entanglement[23]. The viscoelasticity of HA is connected to the molecular weight and concentration[23]. Since the discovery of HA in 1934 its use in biomedical and tissue engineering have expanded greatly due to its many attributes including:

biocompatibility, biodegradablity, chemically modifiable, and non-immunogenic[27, 29]. HA plays a role in tissue growth and remodeling[30], regulation of cell adhesion[26], mediation of cell growth and proliferation, cell motility, extracellular molecular signaling[28], and angiogenesis[21]. HA has a relatively simple structure but can be modified typically at the carboxylic acid or the hydroxyl groups, Figure 4.

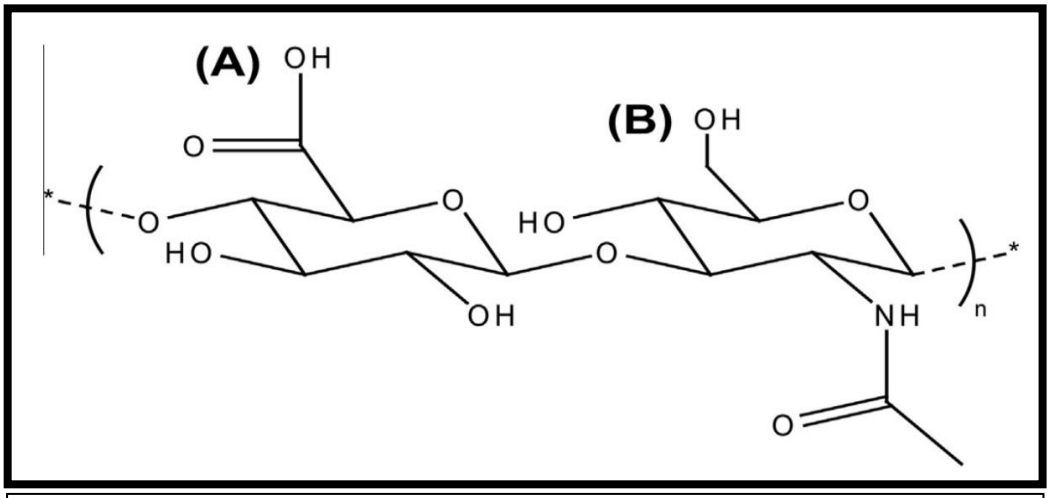

Figure 4. Structure of HA showing possible chemical modification sites. (A) is the carboxylic acid and (B) is one of the four hydroxyl sites. (Reproduced from Muir)[23]

Modification of HA affords the ability to crosslink the normally linear strands and binding of peptides such as arginine-glycine-aspartic acid (RGD), an adhesive peptide to enhance cell binding[24]. HA has a natural CD44 cell receptor that is used to bind to cells in the meniscus[21, 30]. Interactions with the CD44 receptor can play a pivotal role in tissue growth and remodeling[30]. The capability for orthogonal chemistries for HA modification can also allow for multimodal systems: enhanced crosslinking and enhanced cell attachment or signaling[31, 32]. Enhanced crosslinking density can affect mechanical properties of the hydrogel, increasing the strength and compressive moduli and altering the viscoelasticity[25]. Control of the viscous and elastic components of the hydrogel network offers a platform in vitro system to investigate how these properties affect mechanotransduction and the interplay during tissue regeneration.

Viscoelasticity and Mechanotransduction for Tissue Regeneration

As discussed previously, the ECM is a complex environment that is constantly degrading and rebuilding[33] and is an integral part of the interaction with cells to perform fundamental processes such as proliferation, migration, and differentiation[14]. Until recently, these interactions were examined in context of the elasticity of the cellular environment as cells attached to and interacted with the ECM[34]. It is becoming more apparent that the ECM is not a simple elastic system and new and innovative materials are necessary to investigate the importance of the viscoelastic properties of the ECM as it communicates with cells[14]. The fluid nature of the ECM lends to more viscous fluid properties, while still maintaining connection or crosslinks that exhibit elastic components. The viscous components address the time dependent nature of the deformation of the cell attached to the surface[35]. In cartilaginous tissues the loss modulus (viscous components) is 10-20% of the storage modulus (elastic component). This characteristic makes designing hydrogel models that mimic the native ECM more difficult[36], but they are critical for understanding the behavior of cells[14]. The differences of forces that are exerted on the cells effectively transmit mechanical cues to the cells to promote biochemical signaling, a process known as mechanotransduction[37]. Hydrogels with adaptable properties, such as HA, have been utilized to examine dedifferentiation of chondrocytes in the avascular articular cartilage with some success[38] and fibroblast differentiation[39]. Some hydrogels have been modified with the RGD peptide enhancing cell adhesion[40]. Although these studies investigate the effects of viscoelasticity on tissue regeneration are promising, they are still relatively new and limited[14, 41].

Thesis Objectives

The overall purpose of this thesis is to develop a thiol-ene based hyaluronic acid hydrogel network with tunable crosslink density to achieve a range of viscoelastic properties for future characterization of cell phenotypes and behaviors. To accomplish this, the role of degree of ene substitution on network formation and resulting physical properties were investigated. Crosslinked network formation was assessed via the physical properties determined by the swelling ratio, compressive modulus at 10-20% strain, secant compressive modulus, crosslink density, and experimental low field NMR data to show a relative mesh size trend. The results from this thesis will inform future design and fabrication of hyaluronic acid-based hydrogels to investigate the role of viscoelastic properties on mechanotransduction in cells involved in the repair of the meniscus.

Materials

Materials for PHA production

The materials required for production of PHA were as listed below: Sodium Hyaluronate of molecular weight 60 kDa was purchased from Lifecore Biomedical in Chaska, MN. The molecular weight distribution range was listed as 66-99 kDa. 4- Pentenoic Anhydride, 98% was ordered from Sigma Aldrich, St. Louis, MO. N,N Dimethylformamide, (DMF) of 99.8% purity was ordered from Sigma Aldrich, St. Louis, MO. Ultrapure water that was deionized and ultra filtered was obtained from Fisher Chemical, Waltham, MA. Sodium Hydroxide granular crystals were obtained from Sigma Alrich, St. Louis, MO, and dialysis tubing with a mwco of 6-8k was ordered from Spectrum Labs, in Piscataway, NJ.

Materials for PHA Hydrogel Production

The materials required for production of PHA hydrogels were as listed below: DL – Dithiothreitol, (DTT) of >99% purity was obtained from Sigma Aldrich, St. Louis, MO. Lithium phenyl-2, 4, 6 – trimethylbenzoylphosphinate (LAP) of >95% purity was ordered from Sigma Aldrich, St.

Louis, MO. Ultrapure water that was deionized and ultra-filtered was acquired from Fisher Chemical, Waltham , MA. Sodium Chloride small, granular crystals of >99% purity were purchased from Sigma Aldrich, St. Louis, MO. The borosilicate glass plates of 100mmx60mm were obtained from Kennedy Glass in Lawrence, KS. The PLA printed frames with inner dimensions of 20mmx40mmand 1.25mm height were printed on the Monoprice MP voxel #D printer purchased from Monoprice, Rancho Cucamonga, CA. Phosphate Buffered Saline at pH 7.4 was obtained from Gibco, Waltham, MA. The DMEM+ is Dulbecco's Modified Eagle's Medium with addition of penicillin and streptomycin and was purchased from Gibco, Waltham, MS. The penicillin and streptomycin were both added at 1 v/v% and the fetal bovine serum was added at 10 v/v%. These additional media components were also ordered from Gibco.

Methods

Synthesis of Pentanoate Functionalized Hyaluronic Acid

PHA was synthesized, Figure 5, using 60 kDa sodium Hyaluronate (HA) with a listed range from 66 to 99 kDa (Lifecore Biomedical, Chaska, MN). PHA was produced following protocols from[42-45] with modifications as follows:

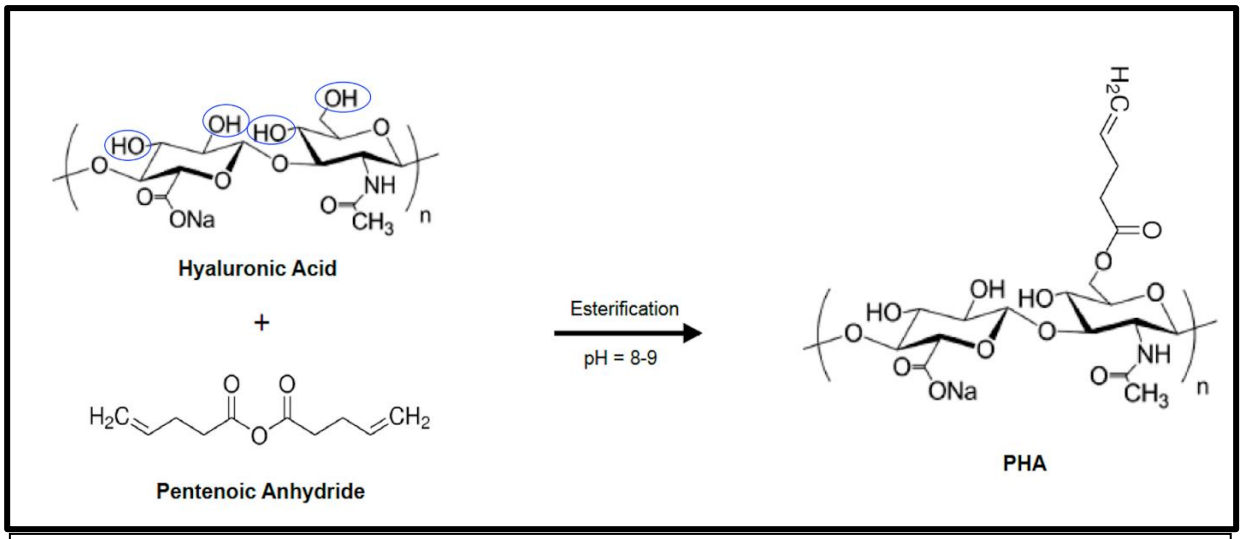

Figure 5. Chemical synthesis pathway of the addition of Pentenoic acid to Hyaluronic acid. (Reproduced and modified from VanKampen 2016)[42]

5 ml of Ultrapure (Millipore Sigma) water was added for each 0.1 g of HA and allowed to dissolve overnight at 4 ˚C. The solution was then transferred to a vertical, tri-neck round bottom flask (24/40) (Millipore Sigma) and stirred with an appropriately sized, oval magnetic stir bar for 60 minutes at 4 ˚C. Stir rate was determined by the position and altitude of the vortex in the reaction vessel. The vortex was optimized to draw down to the stir bar to the point where the stir bar stability was almost disrupted and then back off slightly. This allows for the mixture to aerate the solution with continual mixing and optimal exchange of fluids with agitation by the stir bar. After thorough stirring, addition of N,N–Dimethylformamide (DMF) (Millipore Sigma) (3:2 water:DMF) was performed at a rate of 50 µL every 6 seconds to allow for homogeneous distribution of the DMF in the water. Once addition of DMF was complete, the solution was stirred

for 30 minutes at 4 ˚C to ensure homogeneous mixture of the components. The pH of the solution was adjusted to 9.0 +/- 0.1 using 1 N NaOH and monitoring with a Thermo Orion 420A+ pH probe prior to addition of the next reaction component. 4-Pentenoic anhydride (PA) was then added dropwise, 50 µL/drop, to achieve the desired ratio of PA to the repeating unit of HA. For a 5:1 Molar ratio of PA:HA this equated to 0.24 g of PA added for each 0.1 g of HA added. For the entire addition step, pH was maintained between 8.0 and 9.0 to promote deprotonation of the reactive hydroxyl group. Of note, a brown miscible pentanoate in the DMF phase is observed during addition. Figure 6 shows the DMF phase with less and more optimal mixing.

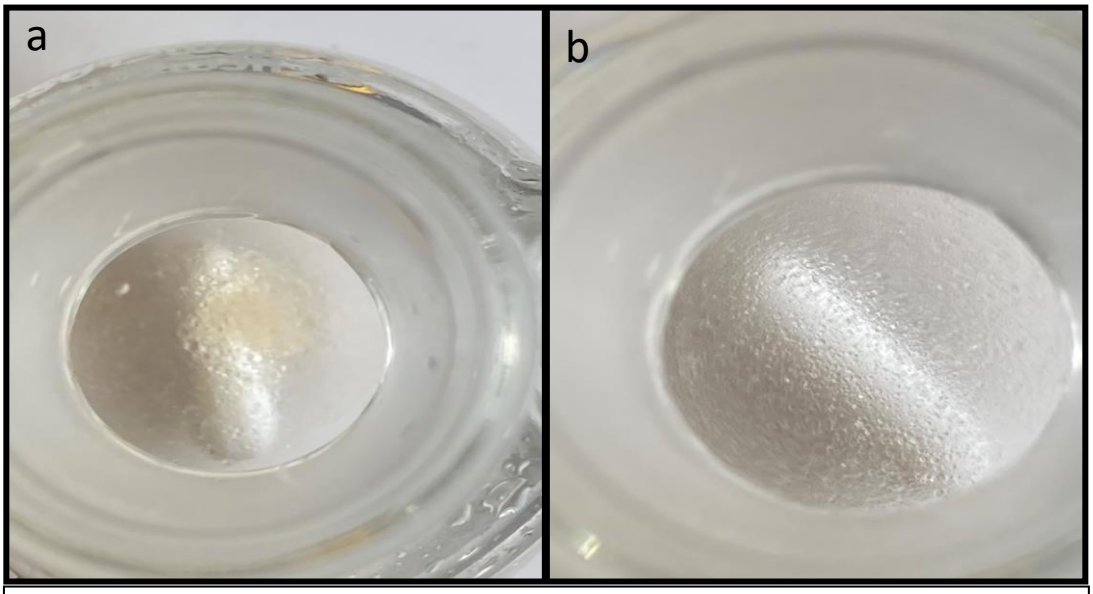

Figure 6. Miscible phase of Pentanoate (PA) in DMF. a.) shows the formation of a brown miscible phase of PA in DMF under less optimal conditions. b.) shows the more optimal distribution of the PA in DMF with mixing that leads to increased reaction rates.

It was discovered that breaking up the brown miscible portion into the smallest droplets allows for increased reaction rates and increased DoS. With optimized mixing and dissolution of the PA in the water:DMF solution the pH was shown to drop from ~9.0 to 8.0 in 15-20s. This increased reaction rate was observed as a determinant of optimal reaction coordinates leading to increased DoS. The majority of the reaction occurred in the first 2 hours after addition of the PA. The

reaction was monitored and pH adjusted for 4-6 hours depending on the rate of pH shift for the reaction. Once the pH shift from 9 to 8 took greater than 30 minutes, the pH was adjusted to 9.5 one additional time and then left to stir overnight at 4 ˚C. Afterward, the pH was adjusted to 8.5 and then the reaction solution was transferred to dialysis tubing with a 6-8 kDa mwco (Spectrum, Repligen Rancho Dominguez, CA) and placed in dialysis against 18 L of diH_2O stirring at room temperature (RT) for 6 hours. At 6 hours, the dialysis was exchanged to new diH_2O. This process was done through 6-8 exchanges over several days. The PHA was recovered from the dialysis tubing, and 25 ml was transferred to each 50 ml conical tubes and frozen at -80 ˚C. The frozen PHA pellets were then lyophilized at -50 ˚C and ~1.5 Pa vacuum using a Freezone 6 lyophilizer (Labconco, Kansas City, MO). The pellets were processed until all water content was removed. The recovered pellets were analyzed by proton NMR to determine the DoS for PA on HA.

Characterization of PHA by NMR

The functionalization of PHA was determined as the degree of substitution (DoS) of the hydroxyl groups of the HA disaccharide repeating unit with PA groups. The DoS was determined through ^{1}H NMR analysis of PHA using an Avance AVIII spectrometer operating at 400 MHz and ~22 ˚C. Samples were prepared by adding 10 mg of lyophilized PHA to 600 µL of deuterium oxide (D_2O, Millipore Sigma) and allowed to fully dissolve. The DoS was calculated by integrating the area under the peak of the double bounded methylene groups from the addition of PA to HA occurring at 5.8 ppm compared to the methyl protons of HA at 2.0 ppm. A reported DoS of 100% denotes that on average one -OH group on each HA repeat unit has a PA group substituted. Figure 7. Overlay of ^{1}H NMR traces for all PHA substitutions. Shown is the chemical structure of PHA with MestReNova predictions of the proton ppm representation for this chemical entity. This shows

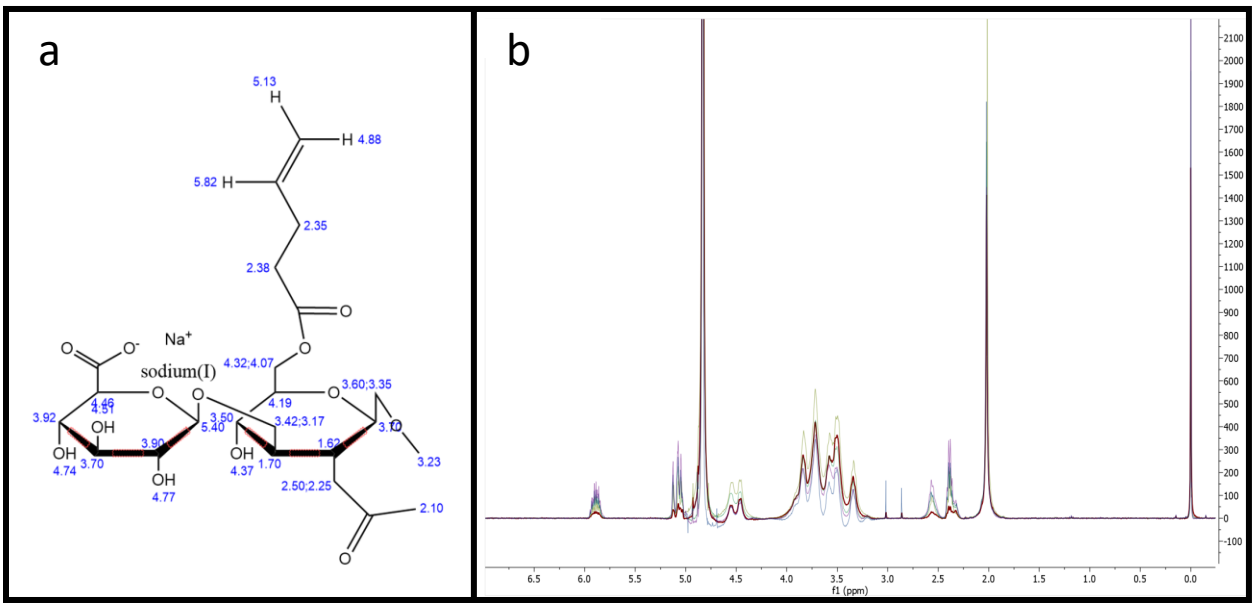

Figure 7. ^{1}H NMR Overlay of PHA reactions and chemical structure of PHA with ^{1}H NMR peak recovery positions, in ppm. a.) illustrates the structure of hyaluronic acid with the substituted pentanoate group. b.) shows the overlay of the ^{1}H NMR traces for all of the molar ratios of HA:PA for the substitution reaction.

that the methyl groups of HA are expected to show at 2.0 ppm and the methylene proton from PHA is expected to show at 5.8 ppm. The overlay shows the similarity in traces for all PHA lots produced. Figure 8 shows the exact protons analyzed for this procedure in the collected ^{1}H NMR graphs. All PHA samples were dissolved in deuterium oxide ($D^{2}O$) containing (Trimethylsilyl)propionic (TSB), which is used to align all traces at 0 ppm. The integration of the area under the peak of the HA methyl protons represents 3 protons. This is used to calculate the

DoS of PHA from the area under the peak of the double bonded methlylene protons of the added pentanoate group.

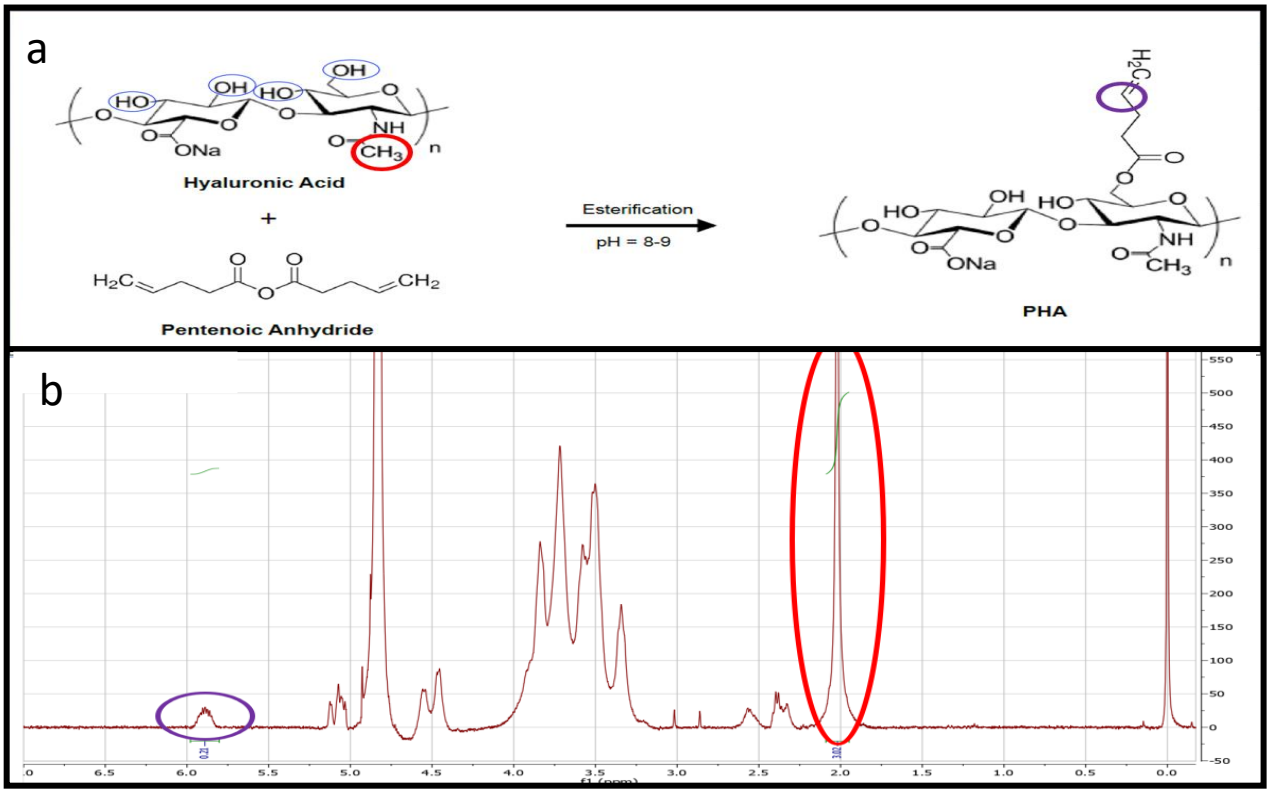

Figure 8 Chemical structures of HA and PHA and ^{1}H NMR trace of PHA. a.) Reaction coordinates for the PHA reaction. b.) ^{1}H NMR trace of a typical PHA reaction product. The peak at 2.0 ppm is representative of the methyl protons of HA, circled in red in both frames. The peak at 5.8 ppm is representative of the double bounded methylene proton of PHA, circled in purple in both frames

Synthesis of PHA Hydrogels

Synthesis of PHA hydrogels, Figure 9, was performed by addition of lyophilized PHA powder to Ultrapure (UP) water containing 0.1 mM of the photoinitiator, lithium phenyl-2,4,6–trimethylbenzoylphospinate (LAP) (Sigma Aldrich). A 1 m*M* LAP stock solution was made and stored wrapped in foil, at 4 ˚C, until required for use in the reaction. LAP was made fresh for each hydrogel production, used within 48 hours of dissolution and was added to a final concentration

of 0.1 m*M* for polymerization reactions. The difunctional crosslinker, Dithiothreitol (DTT) (Sigma Aldrich), was added to the LAP solution at a 1:1 molar ratio of thiol groups to available ene groups on the PHA. PHA was added to the LAP/DTT solution to achieve an 8% w/v% solution. Upon addition of the PHA, the solution was mixed with a microspatula. To remove generated air bubbles, the solution was centrifuged at 7,000 rpm (~2,000xg) using an IEC Clinical Centrifuge (Thermo Waltham, MA) for 90 seconds at room temperature. The solution was recovered and examined to ensure that no air was entrapped in the solution and that the mixture was homogeneous. The mixing and centrifugation process was repeated until all PHA was dissolved and mixed to homogeneity. The PHA solution was then transferred to a 50x36x1.25 mm PLA plate that was adhered to the top of a 105x50x2.3 mm glass plate (borosilicate with no UV protection) with thin application of UP water. The PHA hydrogel solution was transferred using a 1000 µL pipette tip to exclude air entrapment during the pour. The plated solution was then covered with an additional 105x50x2.3 mm glass plate. Clamps were then positioned across the upper and lower glass at the periphery of the PLA form ensuring not to overlap with the PHA solution position during the UV crosslinking step. The poured and plated PHA solution was then transferred to a SpectroLinker XL-1000 UV crosslinker oven (Spectronics Corporation Melville, NY) and irradiated at 312 nm, 3 mW/cm^2 for 300 seconds. The plates were then turned over to expose the opposite side and irradiated for an additional 300 seconds. The crosslinked hydrogels were recovered from the oven and allowed to sit at room temperature for 5 minutes. The top plate was then carefully removed, and the edge of the gel was cut from the PLA form using a razor blade. The PLA plate was removed and the hydrogel on the bottom glass was submerged in a solution of 10 m*M* NaCl in UP water. The gels were allowed to incubate overnight at 4 ˚C prior to mechanical and physical analysis.

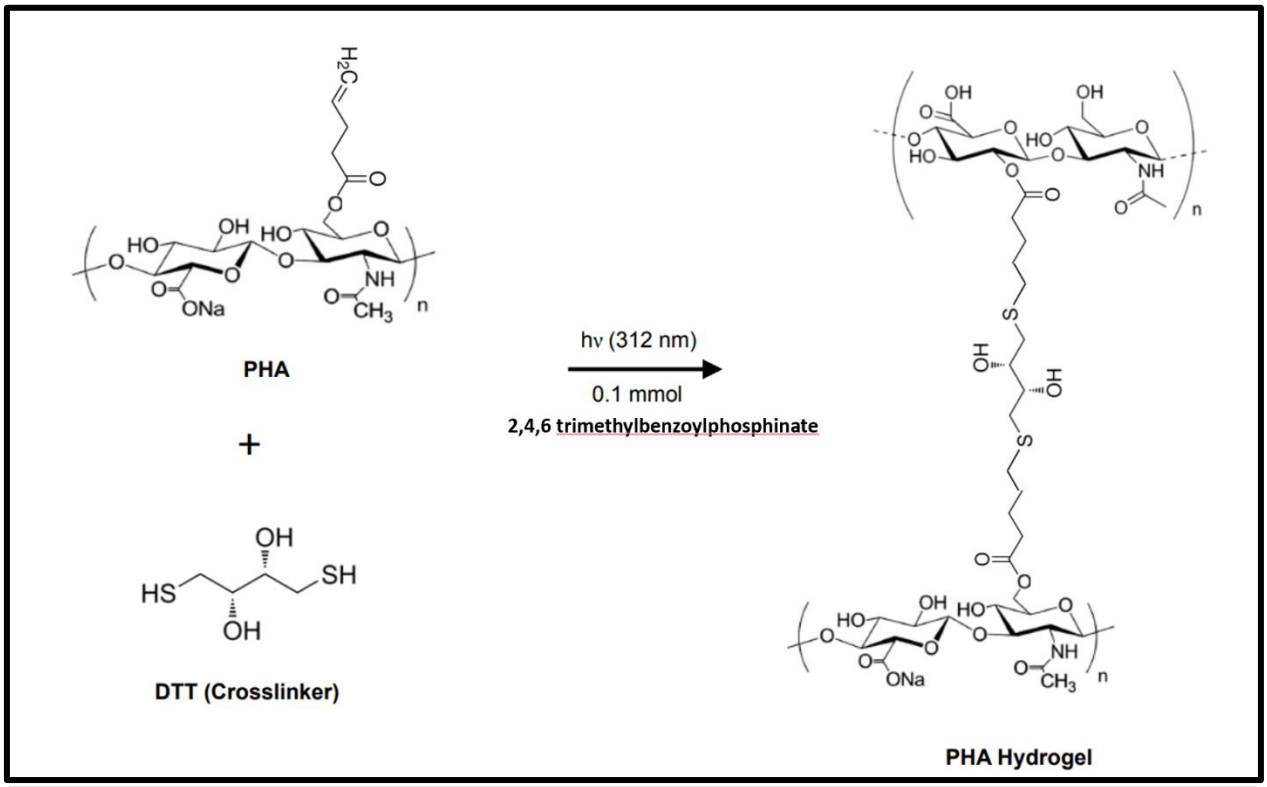

Figure 9. Synthesis of PHA Hydrogels. Crosslinking of pentenoate modified hyaluronic acid occurs via the thiol-ene reaction using the difunctional thiol, DTT, as the crosslinker and lithium 2,4,6 trimethylbenzoylphosphinate (LAP) as the photoinitiator. (Reproduced and modified from VanKampen 2016)[42].

Swelling of PHA (q scores)

8 mm PHA test chips were recovered from either UP water, PBS or DMEM (P/S, FBS) and transferred to 1.8 ml plastic cryovials with snap top caps. The caps had been perforated to allow for air transfer. The tubes were pre weighed and labeled for each sample. The samples were then lightly dabbed on a Kimwipe (Kimberly-Clark, Irving, TX) to remove residual fluids prior to acquiring wet mass weights (m_s) for the samples. Tubes were transferred to a Labconco Freezone 6 (Labconco, Kansas City, MO) and lyophilized at -50 ˚C and ~1.5 Pa vacuum for 24 hours. The

sample tubes with dried pellets were then recovered and weighed to obtain the dry mass weight (m_d) of the hydrogels. Equation 1 was used to calculate the swelling mass ratio, q, of the PHA samples.

$$q = \frac{m_s}{m_d} \quad \text{(Eq .1)}$$

Mechanical Analysis of PHA: Compressive

Compressive mechanical analysis was performed on PHA hydrogels using an RSA-III DMA system (TA Instruments, New Castle, DE) to determine viscoelastic properties of the hydrogel network. PHA cylindrical hydrogel disc, 8 mm, were placed on the 25 mm platen with modified humidity control chamber inline. The platen was lightly coated with mineral oil and zeroed for force prior to initiation of each test. The diameter (mm) for each sample was taken using a digital micrometer (Mitutoyo, Takatsu-ku, Japan). The sample was centered on the bottom platen and the top platen was lowered until 0.5 (g) force was observed on the system. At this point the distance between the lower and upper platen was recorded as the initial height for strain calculations (Equation 2)

$$\varepsilon = \frac{(L_o - L)}{L_o} \quad \text{(Eq. 2)}$$

The test was run to completion at a rate of -0.005 mm/s, uniaxially. The stress-strain curve is used to determine the compressive modulus (E) or the secant compressive modulus (secE). The value for E was determined as slope of the stress-strain curve at strain percentage between 2-10% and also at 10-20%. The value of E from 2-10% strain is further used to calculate the crosslink density (CDL) of the test samples. The value of E from 10-20% is reported as the compressive modulus (E) of the test samples. This follows protocols in literature for materials used in bioengineered samples for cell adhesion studies[41]. The value of the secE was determined as the slope of the

stress-strain curve just prior to the sample reaching initial fracture failure. Although the values for E and secE were determined at different points on the stress-strain curve both utilized Equation 3 to determine the modulus.

$$E = \frac{\sigma}{\varepsilon} \quad \text{(Eq. 3)}$$

Crosslinking Density

Crosslink density for the PHAs of varying DoS was calculated using the affine model, (Equation 4)

$$\rho_x = \frac{G}{RT\,{V_2}^{1/3}{V_{2r}}^{2/3}} \quad \text{(Eq 4)}$$

The model utilizes, G, the shear modulus of the hydrogel to calculate the crosslinking density. For the work in this thesis, the hydrogels were tested in uniaxial compression. The compression data obtains the compressive modulus, E. To find the crosslink density for the hydrogels the value for E is translated into G using Equation 5.

$$G = 1/3E \quad \text{(Eq. 5)}$$

For the remainder of the equation the variables are as follows: R is the gas constant per mole, T is the temperature in K, V_2 is the polymer volume fraction of the hydrogels at testing, and V_{2r} is the polymer volume fraction during hydrogel production. All gels were poured at 8% (w/v) and thus V_{2r} is 0.08 for all calculations. V_2 is calculated from the swelling data averages from the different DoS of PHAs according to Equation 6.

$$V_2 = 1/q \quad \text{(Eq. 6)}$$

The value for q in Equation 6 was calculated from Equation 2.

Frequency Sweep Analysis of PHA

Frequency Sweep dynamic mechanical analysis was performed on PHA hydrogels using an RSA-III DMA system (TA Instruments, New Castle, DE) to determine the viscoelastic properties of the hydrogel network. Cylindrical hydrogels of PHA, 8 mm, were placed on the 25 mm platen, lower, with modified humidity control chamber inline. The platen was lightly coated with mineral oil and zeroed for force (g) prior to initiation of each test. The sample was measured for diameter (mm) using a digital micrometer (Mitutoyo, Takatsu-ku, Japan). The sample was centered on the lower platen and then the upper platen was lowered until 0.5 force (gm) was observed on the system. At this point, the distance between the lower and upper platen was recorded as the initial height for calculating strain (Equation 7) and stress (Equation 8).

$$\varepsilon = \theta K_{\varepsilon} \quad \text{(Eq. 7)}$$

$$\sigma = F K_{\sigma} \quad \text{(Eq. 8)}$$

To calculate strain the component θ is the displacement, and the K_{ε} is equal to 1/L, where L is length (m). To calculate stress the component F is force (g) and K_{σ} is calculated by Equation 9.

$$K_{\sigma} = \frac{G_c}{A} \quad \text{(Eq. 9)}$$

To calculate K_{σ} the components G_c is equal to the gravitational constant 980.7 (cgs) and the component A is area (m^2). The test was then performed under strain control at 1% strain. The hydrogel sample was modulated at frequency from 628 rad/s down to 0.01 rad/s collecting 25 points/decade. This data was transformed using the TA Orchestrator software to calculate E' (storage modulus) Equation (10), E" (loss modulus) Equation (11), and the tanδ Equation (12).

$$E' = cos\delta\left(\frac{\sigma}{\varepsilon}\right) \quad \text{(Eq. 10)}$$

$$E'' = sin\delta((\frac{\sigma}{\varepsilon}) \quad \text{(Eq. 11)}$$

$$tan\delta = \frac{E''}{E'} \quad \text{(Eq. 12)}$$

For E' and E" calculations the component δ is the phase angle, shift between the strain and stress vectors.

Low Field NMR analysis of PHA

PHA polymerized hydrogels were poured according to the procedures discussed previously in this paper. 5 mm samples were collected directly after UV crosslinking and placed in sample containers for the Bruker system or placed in UP water to swell for 24 hours prior to transfer to sample containers to be processed for Low Frequency (LF) NMR analysis. The PHA hydrogel samples were tested at 20 °C using a Bruker (Billerica,MA) Minispec mq-20 operated at 0.47 T and 20 MHz. Transverse relaxation time (T_2) data was obtained via the Carr-Purcell-Gill (CPMG) pulse sequence. A total of 30,000 echoes were collected with a 90°-180° pulse separations (τ) of 0.2 ms and a recycle delay of 10 s, using 4 scans.

Enzymatic Degradation of PHA

Hydrogels from PHA of different DoS values were analyzed for enzymatic degradation by Hyaluronidase (HYAL) using a modified protocol from [46]. HYAL attacks and breaks the glycosidic bond in the backbone of HA, Figure 10. Hydrogel discs, 6 mm, were swollen in UP H_2O for 48 hours. Initial mass was obtained and then samples were transferred to 24-well microplates (Fisher Scientific) with ~500 Units/mL of HYAL (Sigma Aldrich) dissolved in UP

H_2O. This HYAL contains HYAL1 and HYAL2, 2 of the 6 forms of HYAL, but the 2 most commonly found HYALs. Standard addition as described in literature is 50 Units/mL.

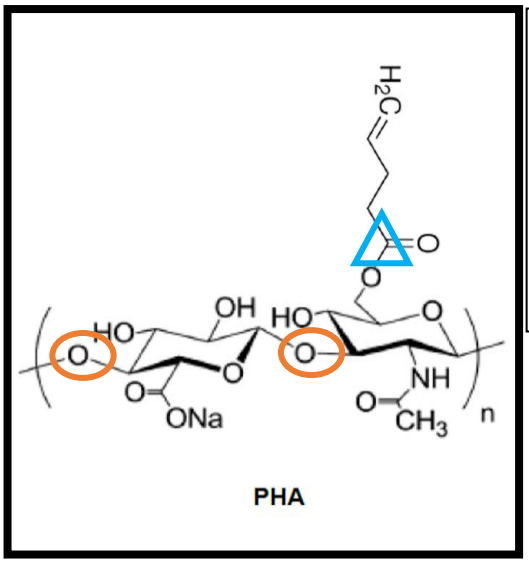

Figure 10. Structure of PHA. The circles represent the glycosidic bond positions that are attacked by HYAL. The triangle represents ester bond that is attacked during hydrolytic degradation.

Preliminary testing showed limited degradation with this amount of HYAL after 3 weeks. To ensure that decay was observed within 14 days the amount of HYAL was elevated 10x. The plate was then transferred to a New Brunswick S41i incubator (Fisher Scientific) set at 37 ˚C with a shaker platform cycling at 100 RPM. The samples were removed from the incubator after 24 hours incubation in HYAL and lightly dried to record the mass of the degrading hydrogels. Once the mass was recorded the samples were replaced in the 24-well plate with a fresh addition of ~500 Unit/mL of HYAL in UP H_2O. This process was repeated every 24 hours on the same samples for 14 days. For each DoS represented, 6 samples were measured until degradation of materials prohibited continued measurements to be recorded (limit of detection set at 30% remaining weight). Controls were run as 4 samples of each DoS represented and were incubated in UP H_2O with no HYAL present, to assess effects of hydrolytic degradation.

PHA Mixture

PHA hydrogels were created as a mixture of two PHA lots to increase the ability to fine tune the PHA network by making any desired DoS inside the upper and lower bounds of the existing PHA DoS values. A low PHA (lPHA) DoS and a high PHA (hPHA) DoS were mixed to create an intermediate PHA. The mixture was calculated as the total number of substitution sites in the desired mixture derived from the weighted averages of the lPHA DoS and the hPHA DoS. The number of monomers is determined for any PHA using Equation 13.

$$Monomers\ (M1) = Da(\frac{1.66*10^{-24}g}{Da})(\frac{mol\ HA}{379.32\ g})(\frac{6.022*10^{23}\ molecules}{mol\ HA}) \qquad \text{(Eq. 13)}$$

The monomer value (M1) for PHA was then used to calculate the number of monomers required to create the desired DoS of the mixture, Equation 14.

$$M1\ x\ desired\ DoS = required\ DoS\ (RM) \qquad \text{(Eq. 14)}$$

The RM is then used to calculate the amount of lPHA and hPHA required to make the mixture at the desired DoS, Equation 15.

$$RM = (M1\ x\ hPHA\ DoS)(wt\%high) + (M1\ x\ lPHA\ DoS)(wt\%low) \qquad \text{(Eq. 15)}$$

For this study a mixture of 47% was produced using a 34% PHA and a 70% PHA. The PHA hydrogels from the 47% mixture were analyzed for Swelling ratio (q) and DMA Compression. The 47% mixture was chosen to have a direct comparison to the 46% PHA that was produced from the 1:3 (HA:PA) molar ratio chemistry detailed previously in this study.

Statistical Analysis

GraphPad Prism 9 was used to perform 1-way and 2-way ANOVA statistical analysis for all data represented in this study. Bonferroni's post hoc test was performed following all ANOVA tests. For analysis of the swelling ratio (q score), the effects of DoS on the swelling of the PHA gels, a 1-way ANOVA was performed. The 2-way ANOVA was performed to analyze the effects of the DoS and media on swelling. In determining the effects of the DoS and media on the compressive modulus 2-way ANOVA was performed. The analysis of the tanδ using the 2-way ANOVA examined the effects of the DoS and the media on the viscoelasticity of the PHA hydrogels. For analysis of the LF NMR results, the 1-way ANOVA was used to analyzed the effect of DoS on the T2 relaxation times. When analyzing the enzymatic degradation of PHA hydrogels with hyaluronidase, a 2-way ANOVA was performed to see the effects of DoS and time on degradation. A 2-way ANOVA was performed to analyze the effects of the DoS and media on compressive modulus for the PHA gels made as mixture versus through the chemical reaction. For this same data, a 2-way ANOVA was also performed to analyze the effects of DoS and media on the swell ratio.

Results and Discussion

PHA chemistry and NMR

Molar rations were modulated in the esterification reaction to fabricate PHA with tunable DoS of reactive ene groups. Figure 11 shows the chemical structure of PHA and the predicted peak positions for the protons of PHA alongside a typical spectrum recovered from NMR analysis using MestReNova software. The area under the curve for the 2.0 ppm shift representing the methyl protons of HA was integrated and standardized for 3 protons. The area under the curve at 5.9 ppm was integrated and calculated using the standardized value of the area under the curve at 2.0 to determine the DoS of PA onto HA. A DoS of 100% denotes that one PA moiety was substituted for every HA monomer. As each HA monomer has 4 hydroxyls available for potential substitution a 400% DoS is the maximum possible, although highly improbable. Table 1 shows the results for DoS for the lots of HA that

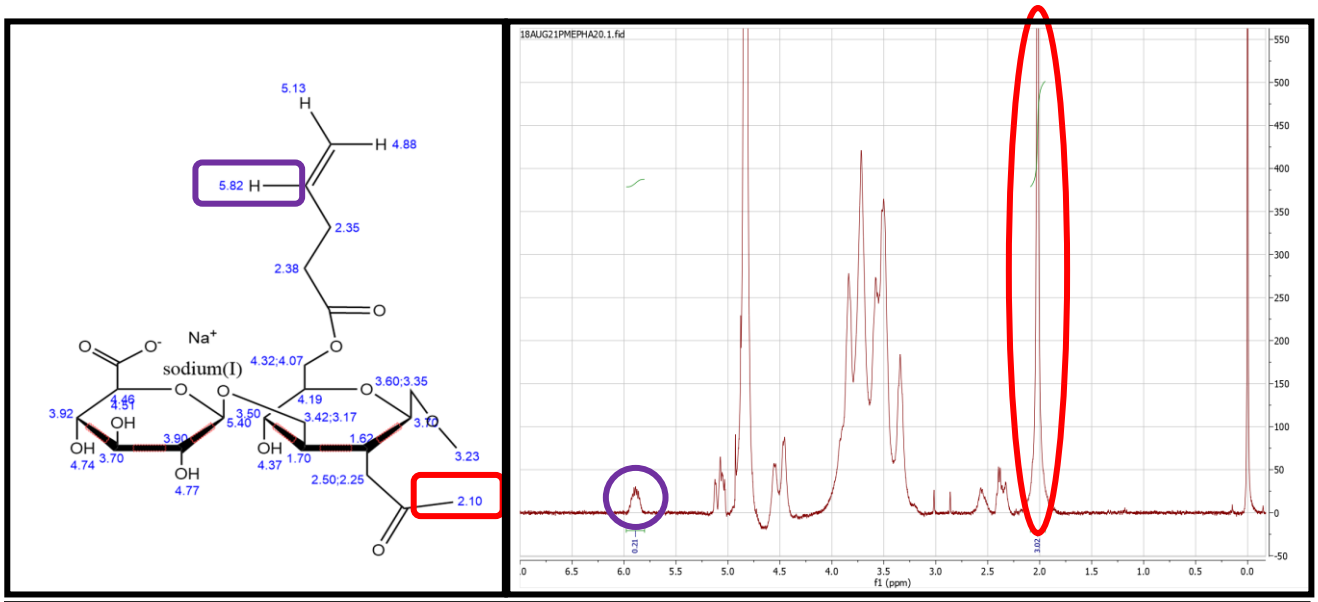

Figure 11. Pentenoate functionalized Hyaluronic Acid (PHA) chemical structure and ^{1}H NMR graph of typical PHA sample. The left panel depicts the predicted peak alignment for all PHA protons. The right panel is the graph of ^{1}H NMR for PHA. The 5.82 ppm peak, purple box, methylene proton and the 2.10 ppm peak, red box, methyl protons are the peak areas that will be used to calculate DoS for PHA.

were modified with PA at the variable ratios. Three reactions were performed at a molar ratio of 1:1 resulting in 22, 23 and 22% DoS. Two reactions were performed at 1:3 and 1:4 ratios resulting in 46% and 47% and 65% and 70%, respectively. A single reaction was performed at 1:2 and 1:5 ratios and resulted in 34% and 90%, respectively.

Table 1. Substitution rates of Pentenoate functionalized Hyaluronic acid (PHA).

Molar Ratio HA:PA	Degree of Substitution
1:1	23%, 22%, 22%
1:2	34%
1:3	46%, 47%
1:4	65%, 70%
1:5	90%

All reaction products were tested by NMR. Figure 12 shows the NMR overlay graph of these products. The traces show that the peaks recovered for each reaction were similar. Figure 13 shows the expanded view of the overlays of the 5.9 ppm peak. This data exhibits that as the relative moles of PA was increased, the area under the peak increased. The data supports that increasing the molar ratio of PA to HA produced an increase in DoS, as seen by the increased area under the curve for the 5.9 ppm peak. The data also illustrates the reaction as performed was robust and reproducible.

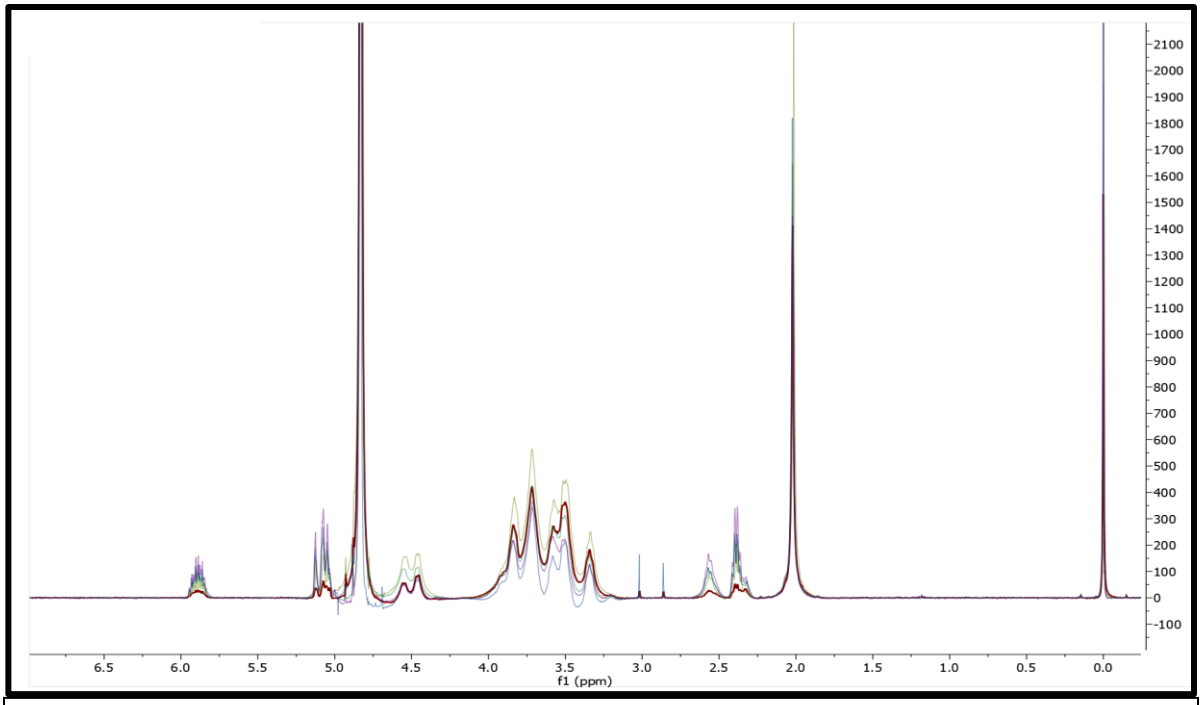

Figure 12. Overlay Traces for ^{1}H NMR of all PHA lots.

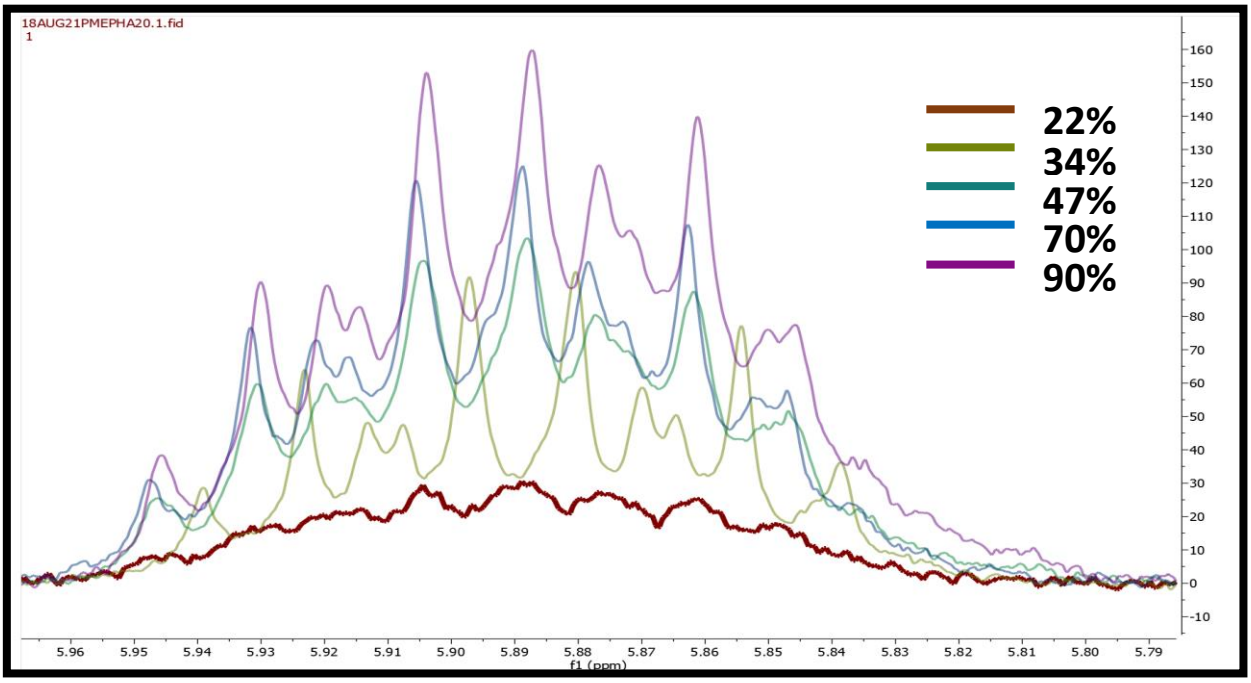

Figure 13. Expanded view of the 1H NMR traces for each DoS of PHA.

Swelling mass ratio (q)

PHA samples were swollen in UP water, PBS or DMEM+ and then dehydrated to assess the swelling capacity for each sample in the different solutions. Figure 14 shows the average swelling mass ratio (q) values for the PHAs at varying DoS. In UP water, the hypothesized decrease in swelling with increased crosslink density via the increase in DOS was observed. Significant differences were seen between the hydrogels fabricated at 22% DOS compared to 34 and 90% DOS. The PHA at 46%, 68% and 90% in UP water do not show significant differences in their swelling mass ratios. Further, PHA samples in UP water are significantly more swollen at lower DoS than any of the PHA samples in PBS or DMEM. The PHA samples swollen in PBS and DMEM+ did not show any significant differences in swelling at any of the DoS values.

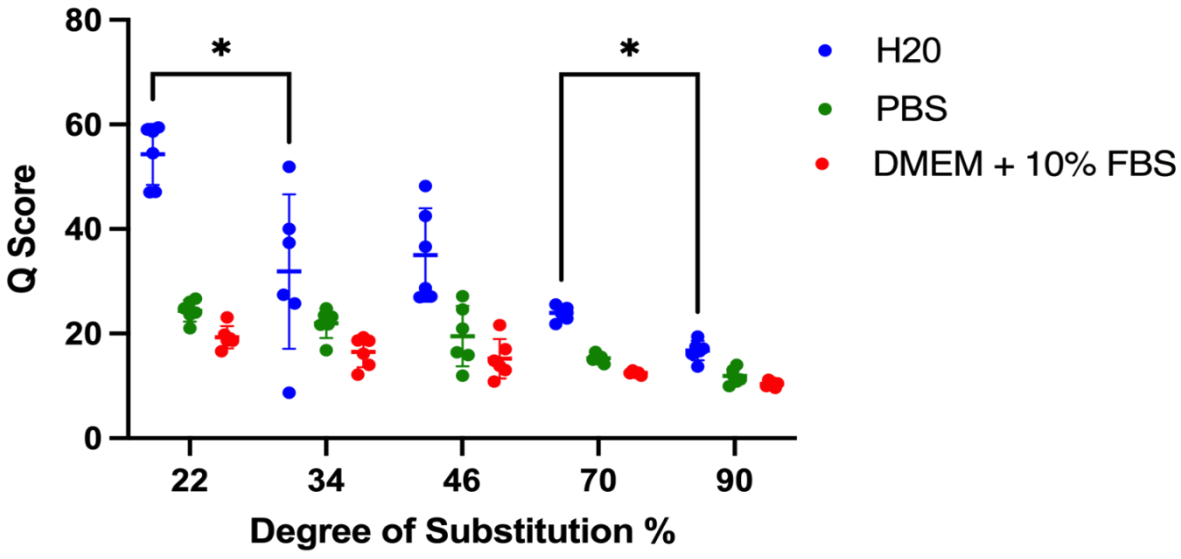

Figure 14. Swelling mass ratio (q) for PHAs of varying DoS in UP water, PBS, and DMEM+.

The data indicates that PHA samples swollen in water are linked to DoS; the lower the DoS the higher the q score, and the more the gel swells. Whereas the PHA samples in PBS and DMEM+ do not follow the same trend. These samples have limited swelling capability in the buffers that have ionic contributions from salt, proteins, and amino acids. The data supports that ionic strength of the buffers generates an osmotic pressure that induces water flow out of the hydrogel with the concentration gradient which leads to osmotic deswelling of the samples[47, 48]. This effect outweighs the contributions to swelling seen with increasing DoS. Considering that future work will be performed for cell culture in DMEM+ media, the lack of variation in swelling may lead to limited tunability of the viscoelastic properties of the hydrogel network. Swelling is critical for diffusion of small molecules. In order for cells implanted in the gels to access nutrients and filter out waste and byproducts from the gel environment diffusion must be effective. Control of the swelling ratio can also lead to control of degradation important for ensuring gels remain intact long enough to support cell adhesion and mechanotransduction. Obtaining more data on PHA gels across broader ranges of swelling, DoS, and buffer conditions is important when considering supporting future mechanotransduction and stress-relaxation studies using PHA gels.

PHA Compression Analysis and Crosslink Density

PHA Hydrogels with increasing DoS were analyzed by compression to assess the elastic moduli. The ratios are the same as was described in the previous sections. Figure 15 shows a typical graph recovered from a compression test of PHA run on the RSA III DMA system and illustrates the different regions that were utilized to calculate the various moduli.

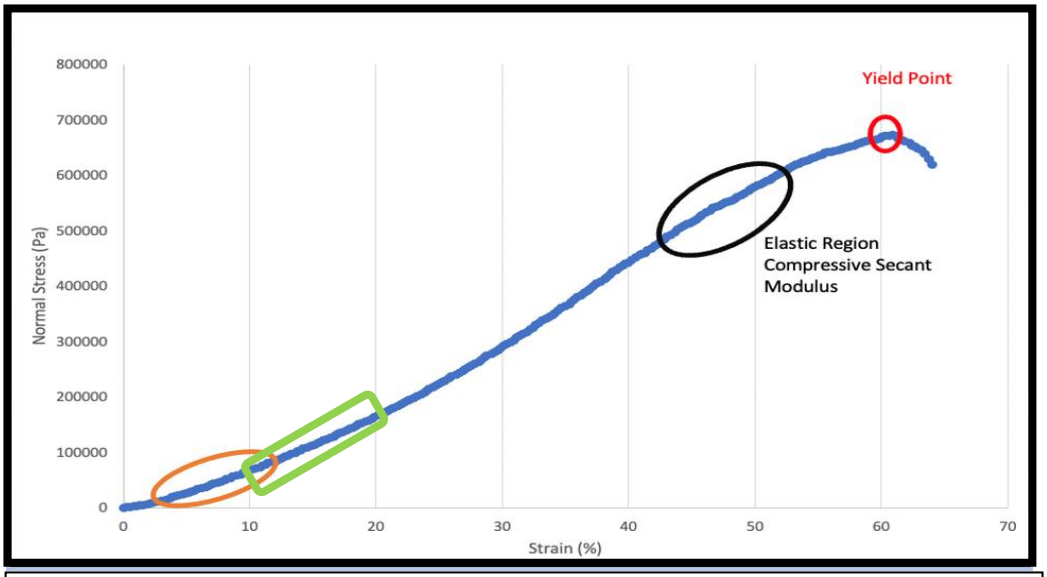

Figure 15. Stress versus Strain(%) curve from DMA in Compression for PHA. Shown is a typical graph recovered from the compressive analysis of a PHA test article. . The blue line is the graph of the strain (%) versus stress of the PHA during compression. The red circle outlines the yield point. The orange outline denotes the compressive modulus in the fully elastic region that was utilized to calculate crosslink density of the PHA gels.. The green outline denotes the area between 10-20% strain where the compressive modulus, E, is determined. The black circle denotes the position just before failure where the stress-strain is analyzed to determine the secant compressive modulus, secE.

Each will be addressed individually, however, it should be noted that the region denoted in orange represents the “fully elastic” compressive modulus E, the region denoted in green represents the

10-20% compressive modulus E, and the region denoted in black represents the secant compressive modulus (secE).

Figure 16 shows the overlay of the stress-strain curves for PHA across all DoS. The data shows that as DoS increases the E increases.

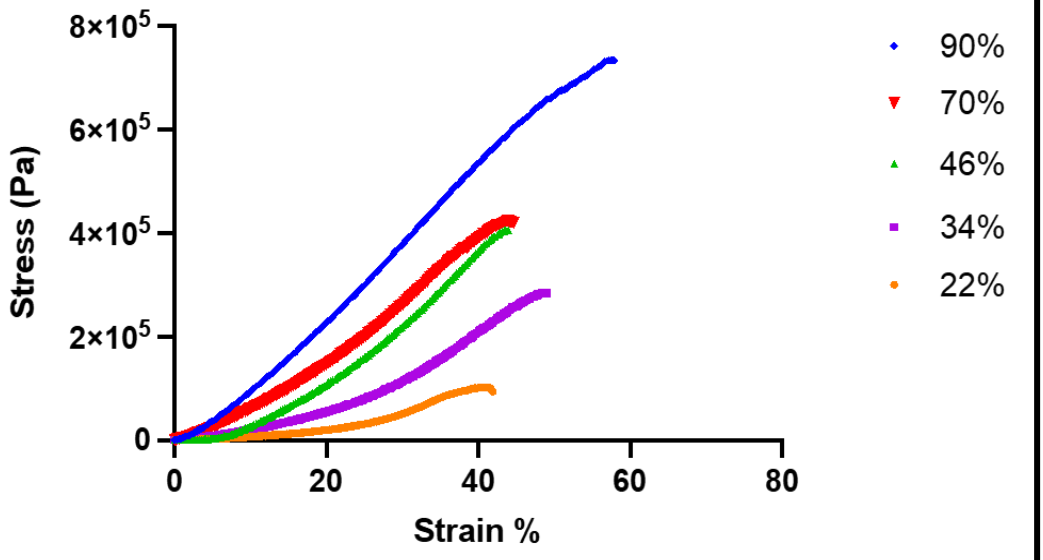

Figure 16. Stress-Strain plot of representative PHA for all DoS.

The region identified in the orange circle in Figure 15 is the 2-10% or "fully elastic" strain region. The compressive modulus, E, was calculated in this region and used to calculate the crosslink density of the PHA gels as previously described. Figure 17 shows the crosslink densities for PHA gels of varied DoS in UP water. The data shows that the crosslink density increases as the DoS increases.

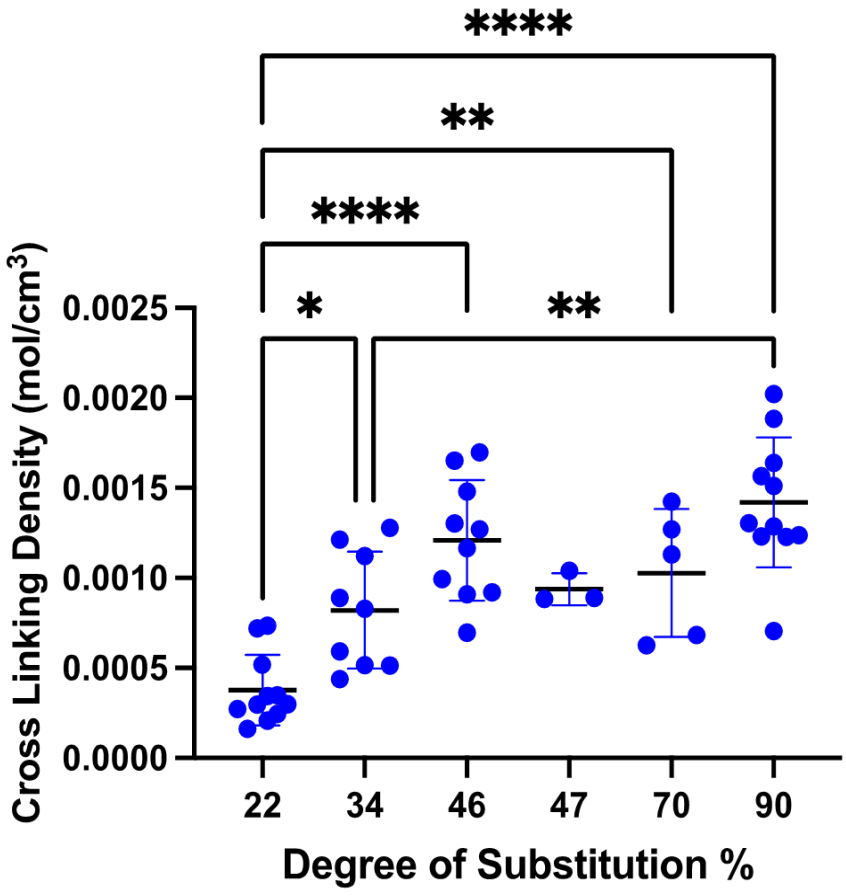

Figure 17. Crosslink Density of PHAs of varied DoS in UP H_20.

The secant modulus analysis is not the same as the compressive modulus, sometimes labeled as the Young's modulus. The compressive modulus is taken early in the stress/strain curve when the hydrogel is asserted to be best fit to the neo-Hookean model for crosslinked polymers. This data does not address the neo-Hookean model, but rather is looking at the maximum compressive modulus prior to fracture.

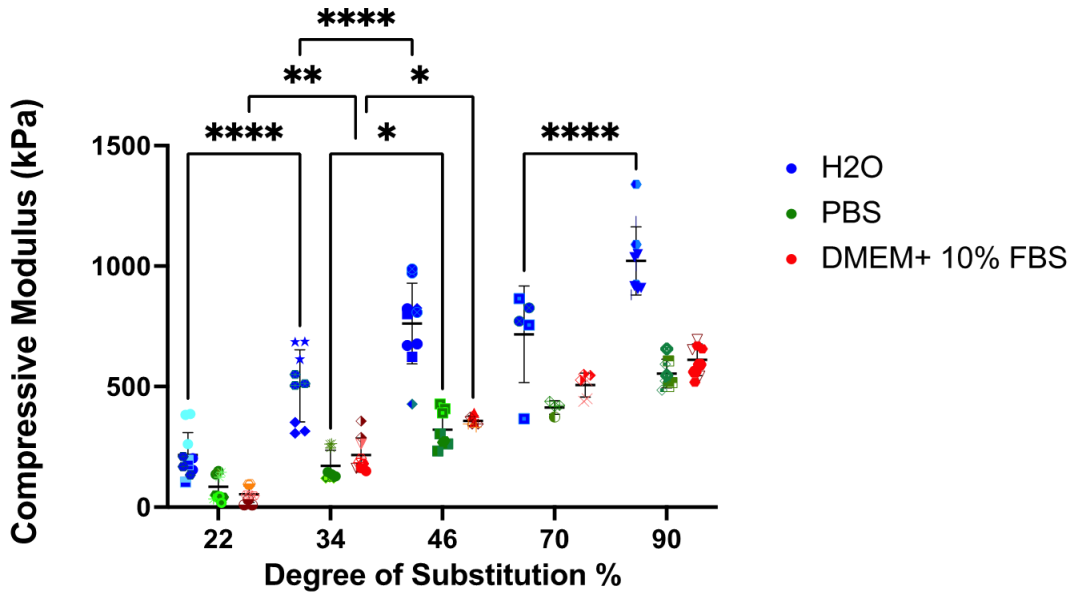

Figure 18. Compressive Modulus at 10-20% strain for PHA of varied DoS in UP H20, PBS and DMEM+. The data represented in blue is for PHA in water, red is in PBS and green is DMEM+. In all groups the varied icons represent gels tested from different lots produced at the same DoS

The region identified in the green square in Figure 15 is the compressive modulus, E, evaluated in the 10-20% strain portion of the curve as is typically calculated in stress-strain analyses and performed in similar hydrogel systems[41]. Figure 18 shows the data for E in this region with different buffers represented in blue, green and red and different lots produced at the same DoS represented by varied icon shapes. The PHA gels do not exhibit behavior that models directly to the classic neo-Hookean model, therefore, this region is utilized to investigate hydrogels that are being used in cellular interaction studies. The values represent material properties experienced by cells as the data (and hydrogel) remains in the elastic portion of the gels. This evaluation also minimizes the noise seen in the initiation of the compression test. The data from Figure 18 illustrates that E increases as DoS increases. The changes of E for PHAs swollen in water are greater than those observed in PBS and DMEM+, which is also likely a result of osmotic

deswelling in the ionic buffers. This shows that in the elastic region of the gels the compressive modulus is directly affected by the number of crosslinks. It should also be noted that a certain degree of variability is expected between different lots of the same DoS. However, the data shown in Figure 18 emphasizes the low level of variability for samples within the same lot, indicting that this data has a high level of reproducibility.

The region circled in black in Figure 15 is the area directly prior to the yield point of the gels. The slope of the stress-strain gives the secant compressive modulus (secE). For analysis of the secE, only the data directly prior to fracture is utilized. The secant compressive modulus is taken as the slope of the stress/strain curve in the elastic region for a particular strain range. For this study, secE was determined by finding the point of fracture and then using the slope that spans a 5-10% range several percentage points prior to fracture. The gel is not fully elastic in this region and has begun to undergo plastic deformation indicating that another, earlier, modulus will likely be more descriptive of the elastic properties of the hydrogel. This area was investigated to determine how drastically the gels changes under extreme strain and how behavior is affected by increased crosslinking. Figure 19 shows the secant compressive moduli of the PHA samples of varying DoS and in the buffers assessed in this study. It is apparent from this data that secE for the PHAs in water increases as the DoS increases. This is a greater change at the lowest DoS and becomes more gradual as the DoS increases. Above 46% DoS the change is minimal. This may be due to the reduction in efficiency of thiol-ene crosslinking and the increase in ene-ene linkages. The secE of the samples in PBS and DMEM exhibit a much different trend, they are elevated at lower DoS compared to those reported in water and remain similar across all groups. This effect is due to osmotic deswelling of the hydrogels in the buffers containing ionic components. The data from Figure 16 shows that the secE within a batch was precise and

reproducible, and that the main source of variance is attributable to the difficulties presented in producing robust hydrogels from batch to batch.

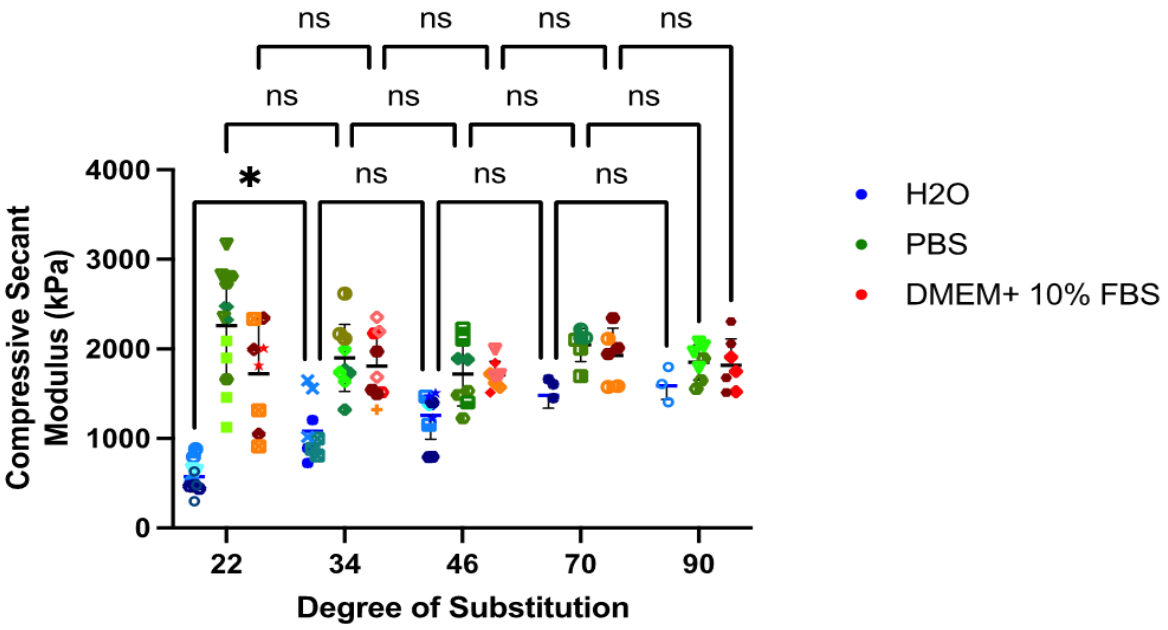

Figure 19. Compressive Secant Modulus for PHA of varied DoS in UP H20, PBS and DMEM+. The data represented in blue is for PHA in water, red is in PBS and green is DMEM+. In all groups the varied icons represent gels tested from different lots produced at the same DoS.

A significant increase in compressive secant modulus was observed for hydrogels tested in UP H2O for DoS at 22%, 34% and 46%. After reaching 46% DoS, modulus values plateau and there is no statistical significance between 46% and 68% or 90%. This plateau is also shown in the calculated crosslink density values for the different DoS samples. The data supports that increased DoS leads to increased crosslinking during polymerization of the hydrogel and increases the strength and rigidity of the gels, but only to a certain degree. At this point it is clear that the chemistry has reached its maximum efficiency within these experimental parameters.

A DoS of 22% is equivalent to having a pentanoate moiety substituted to one -OH site per every fourth HA monomer. A DoS of 46% is equivalent to having a pentanoate group substituted on one -OH site every other monomer. A DoS of 90% is equivalent to having a pentanoate group substituted on one -OH site every monomer. Thus a 90% DoS gel has four times the available crosslinking sites compared to a 22% gel, and between the 22% and 90% the compressive secant modulus increases from ~500 kPa up to ~1800 kPa. Interestingly the 90% DoS gel has twice as many crosslinking sites as the 46% gel but compressive secant modulus only increases from ~1500 kPa to 1800 kPa. The lack of comparatively similar increases at different DoS may be explained by the ability of the gel to crosslink efficiently as the DoS increases. This explanation is supported by the calculated crosslink density values provided in Figure 17. During the crosslinking reaction the formation of crosslinks can lead to steric hindrances in the system and make it increasingly more difficult for the still available sites to be able to link to one another. While the system is not fully optimized the limitations are routinely observed and attributable to common occurrences in polymer chemistry.

Data also shows distinct differences in the compressive secant modulus values between PHA in UP H2O and the other buffers, PBS and DMEM+. Compressive secant values are significantly different at the lower DoS rates and the degree of difference between values diminishes as the DoS increases. When comparing the values of the compressive secant modulus for PHA of any DoS in either PBS or DMEM+ there are no significant differences between the non-H2O groups. This data may indicate that ionic interactions of the buffers outweigh the impact of the crosslinking from the pentanoate sites that were substituted on to the HA. This is a key difference relevant to using these hydrogels in a biological system where the ionic distribution of the fluids would mimic that seen in either PBS or DMEM+. Importantly, in the highly ionic solutions the compressive

secant modulus is maximal at all DoS values indicating an increased strength and rigidity would be observed for even the lowest substitution rates. The downside to this observation is that the tunability of the system appears to be minimized. Overall, increasing DoS in this PHA system increases crosslink density and increases E in all buffer systems.

PHA Frequency Sweep Analysis

PHA hydrogels composing different DoS were analyzed by DMA frequency sweep under strain-controlled conditions to assess storage modulus, loss modulus and tanδ. DoS levels of analyzed samples were the same set that as analyzed throughout all data sets in this study. Figure 20 shows a representative plot of storage modulus (E'), loss modulus (E''), and tanδ during the frequency sweep test of PHA run. All runs were performed on the RSA III DMA system and measurements performed in H2O, DMEM, and PBS buffers.

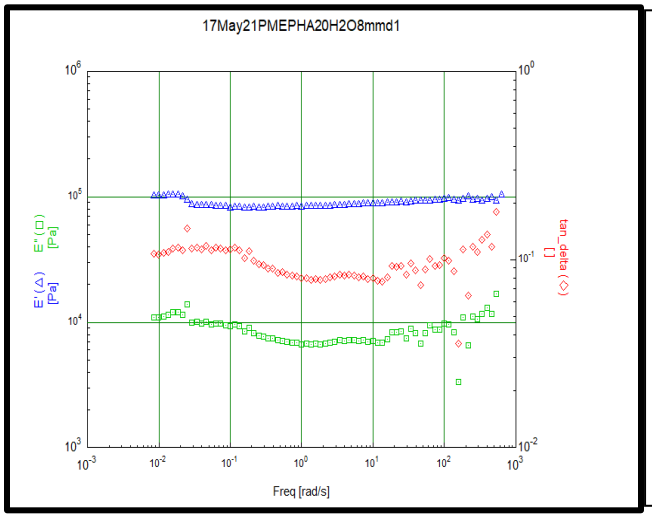

Figure 20. Frequency sweep analysis of PHA. Shown is a typical graph recovered from the frequency sweep analysis of a PHA test article. The blue data represents the storage modulus (E') data at subsequent points across the frequency range tested. The green data represents the loss modulus (E") data for the same frequency range. The red data represents tanδ (E"/E'). The frequency sweeps were run from 628 rad/s down to 0.01 rad/s. This data was consolidated to show the E' and E" at 1 Hz (6.28 rad/s) only.

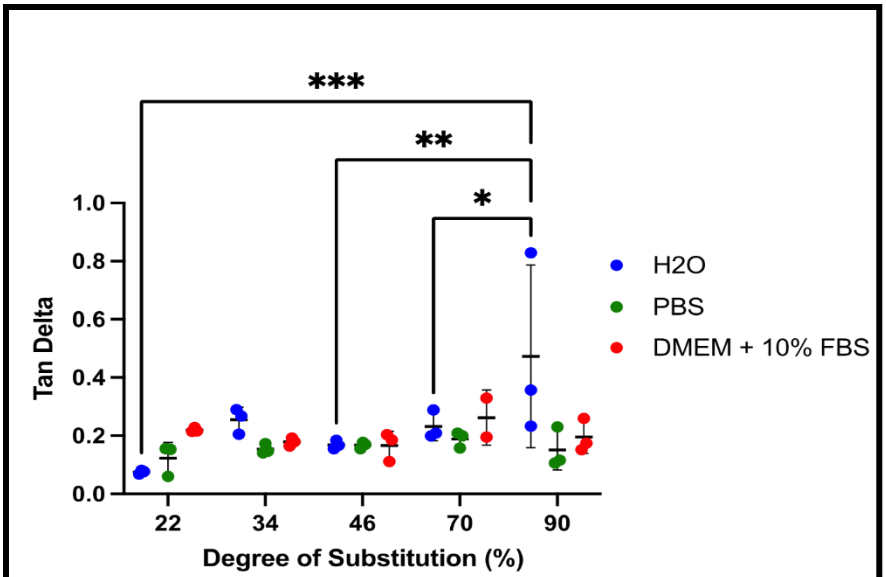

Figure 21. Tanδ versus DoS for PHAs in various buffer conditions.

Figure 21 shows Tanδ versus DoS for PHAs in the different buffer conditions. The data exhibits how the loss modulus increases as DoS increases. This is beneficial for future studies to control the viscosity of this PHA system. Figure 22 shows the frequency sweep results for the PHA DoSs in UP H2O. The graph reports the storage modulus (elastic component) on the x-axis and the loss modulus (viscous component) on the y-axis.

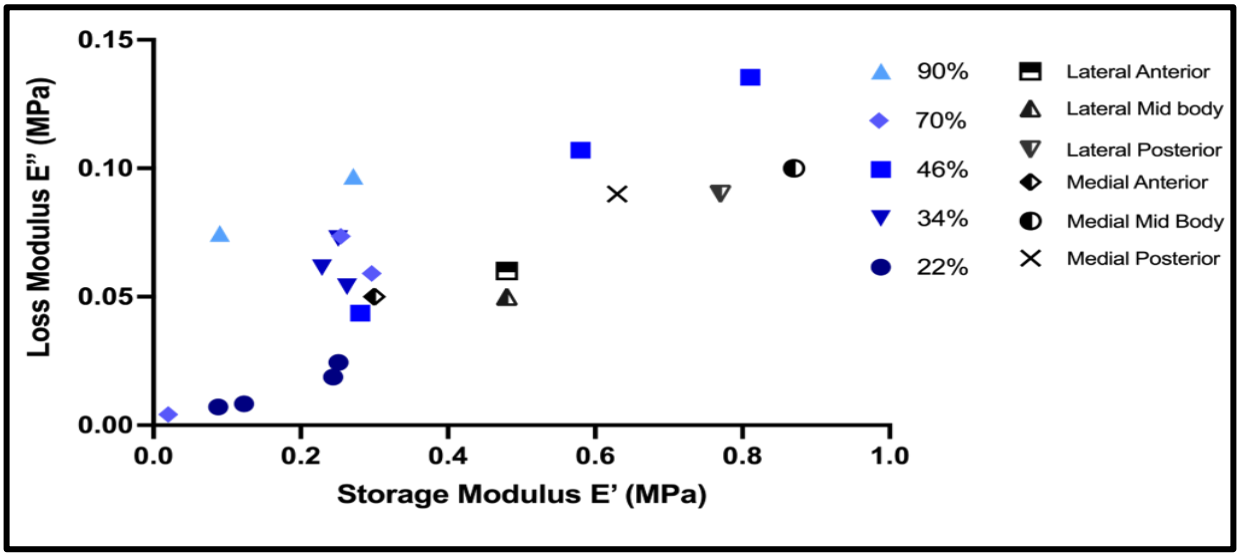

Figure 22. Frequency sweep data from DMA of PHA in UP H2O at 1Hz. Comparison of the E' and E" as a position of DoS.

Results shown in Figures 22, 23, and 24 are data collected at 1Hz, utilized as it is a safe approximation of input seen by the meniscus under normal walking conditions[14]. The data in these figures is represented similar to data from Chaudruri et al where the values for storage and loss modulus of biological tissues, such as meniscus, are shown in this format[14]. The data supports that hydrogels fabricated from PHA exhibit a shift in viscoelasticity that can be correlated to different processing parameters. The increase in crosslinking is correlated to an increase in elasticity. The 22% gels in UP H2O have a E' of around 8 times the E", 200,000 Pa versus 25,000 Pa. The 34% and 68% gels are similar in having E' at 250,000 Pa and E" at 60,000 Pa. The 46% and 90% have highly variable values but overall data sets show increased E' and E" values respectively. The 90% gel ranges from 100,000 Pa E' and E" all the way up to 700,000 Pa E' and 150,000 E". This difference in E' and E'' data could be a combination of increased entanglement that allows for more viscosity and increased crosslinking to give a more solid elasticity portion of the gels. Cartilage viscoelasticity normally exhibits loss moduli that are 10% of its storage moduli, in soft tissues this relationship can be as much as 20%[14]. The PHA gels in this study show to be similarly aligned when comparing E" to E' across the DoSs tested. As a viable model system, the values for the storage and loss moduli are within the range for soft tissue as DoS is increased. As DoS is increased the gels exhibit greater loss, at the tested frequency. This would indicate the gel can dissipate more energy as the crosslinking (and DoS) of the gel increases.

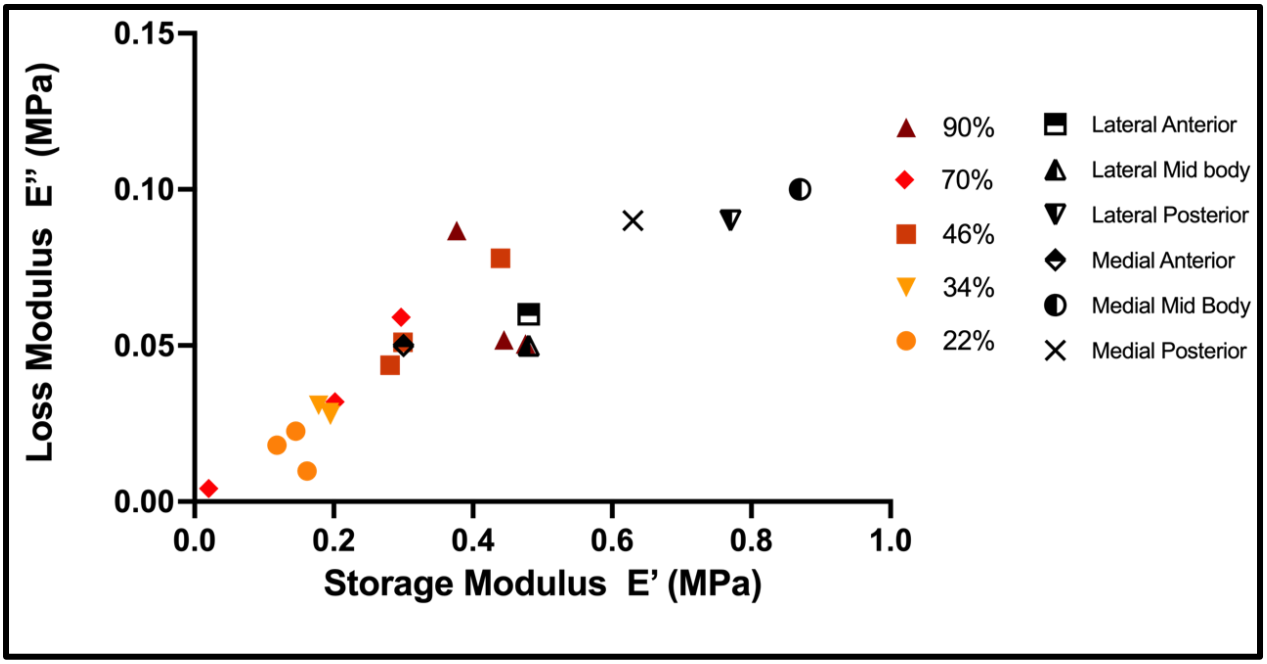

Figure 23. Frequency sweep data from DMA of PHA in PBS. Comparison of the E' and E" as a position of DoS.

Figure 23 shows the frequency sweep results for the PHA DoS in PBS and Figure 24 shows the same data for the PHA in DMEM+. The data is reported in the same manner as Figure 22. The storage modulus (elasticity) on the x-axis and the loss modulus (viscosity) on the y-axis.

The frequency sweep data in PBS demonstrates similar performances of the PHA gels across the tested DoS with the exception that the initial E' trend higher across the spectrum, whereas the E' data is contained across a range of lesser values overall. The 22% DoS gels still group at the lower end of E' and E", 150,000 Pa and 20,000 Pa respectively. The 34% DoS gels are slightly elevated compared to the 22% gels and show at 200,000 Pa for E' and 30,000 Pa for E".

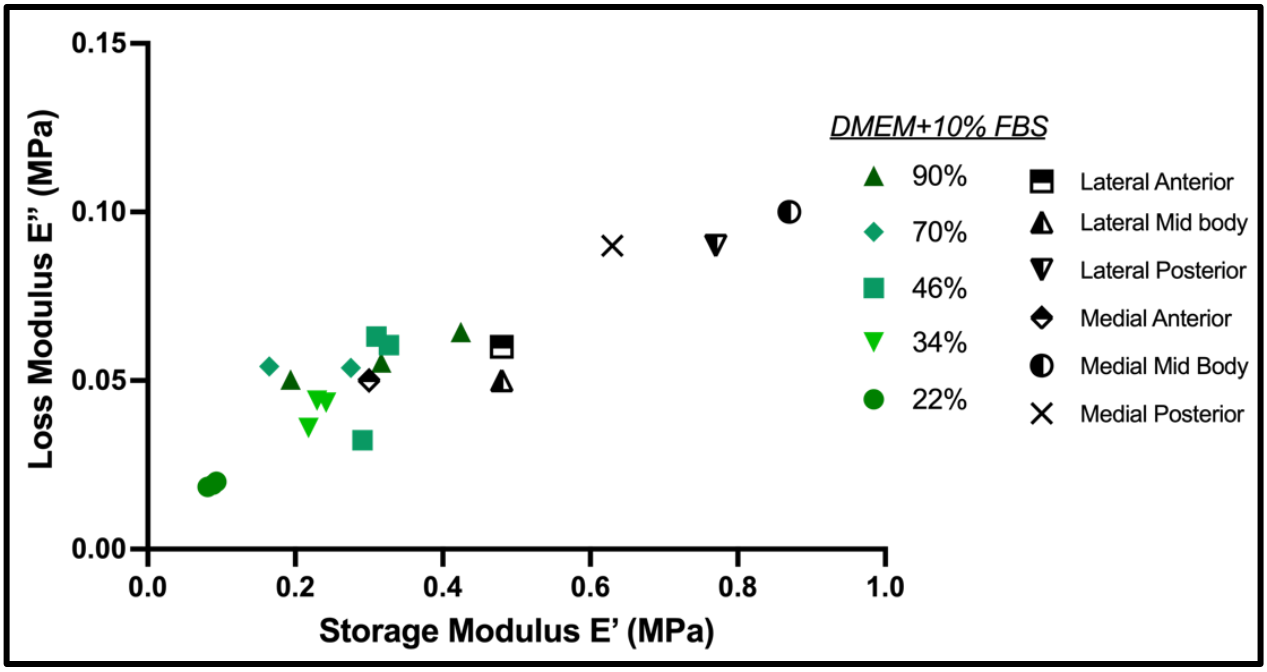

Figure 24. Frequency sweep data from DMA of PHA in DMEM+. Comparison of the E' and E" as a position of DoS.

The 68% gels are again spread out across the graph and range from very low E' and E' up to 300,000 Pa for E' and 60,000 Pa for E". The 46% and 90% gels show tight grouping and are at the top end of the graph. The 46% gel has E' values around 300,000 Pa and E" values at 60,000 Pa. The 90% gels show E' at 450,000 Pa and E" between 60,000 and 80,000 Pa. Overall, the frequency sweep experiments provide key information on material performance and indicate that further investigation of PHA properties in ionic buffers will be necessary in the future.

Low Field NMR

Carr-Purcell-Meiboom-Gill experiments using Low Field NMR[49] were performed on 5 mm PHA samples with the same varying DoS used in prior experiments. The samples were analyzed for the transverse relaxation time (T_2) of the water protons inside the network. Figure 25 shows the data recovered from these experiments.

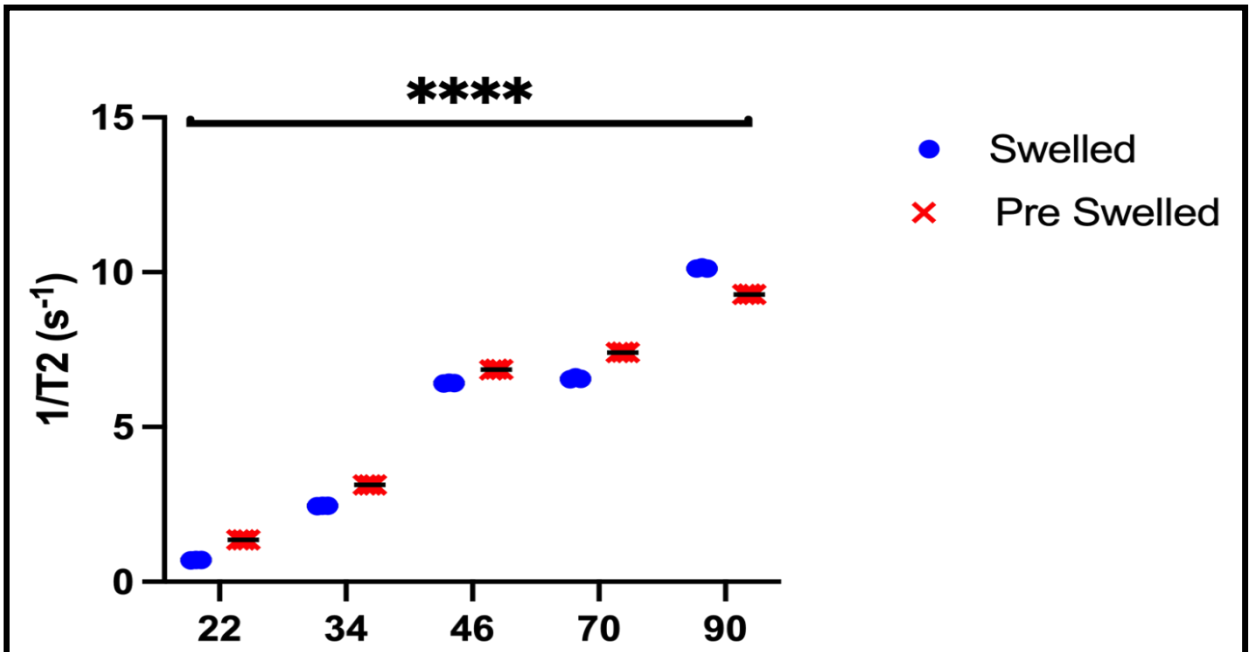

Figure 25. Low Field NMR $1/T_2$ times for PHA hydrogels of varying DoS. The samples prior to swelling are shown in red and the samples after swelling are shown in blue. PHA samples swollen in UP water.

Figure 26 shows the comparison of the same data analyzed in Figure 25. In Figure 26 the data has been standardized, in the panel labeled a) as the inverse relaxation time. This adjustment portrays the data on the same scale and shows that the relaxation shift is the same for both the crosslinked and swollen gels. As the DoS increases the inverse relaxation time goes up. The panel labeled b) shows the change in T_2 at each DoS as a percentage change. This illustrates that at the lowest DoS there is a near doubling of the relaxation time and as the DoS increases this difference is minimized. The effect is that as the DoS increases the gels swell less and effectively the mesh

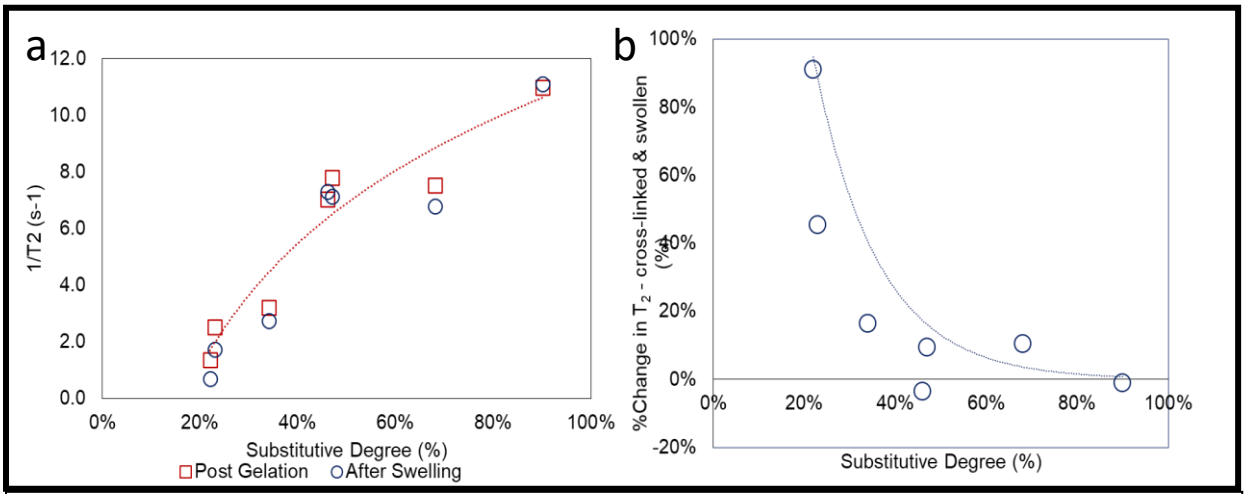

Figure 26. LF NMR data of $1/T_2$ and ΔT_2 graphs of PHA DoS samples in UP water. Panel a) is the inverse T_2 comparison of swollen and unswollen PHA gels. Panel b) is the change in T_2 of PHA gels between pre and post swell states.

size stays more constant. This conclusion aligns very well with the results from the Swelling Ratio results discussed earlier. The higher the DoS the lower the T_2. This also fits well to the hypothesis that increased DoS leads to increased crosslinked density in the gels. Significant differences were observed between all samples other than the 46% and 70% gels after swelling. The swollen 46% and the swollen 70% gels did not exhibit significant differences in relaxation time. The crosslinked gels reported relaxation times that were approximately half of the times reported for the swollen gels. Considering that accurate diameters of HA for the tested samples were not evaluated, it is not possible to generate accurate mesh sizes for the PHA gels. Thus, the data can only be assessed to show that the increase of the DoS leads to greater interactions of the water with the polymer, either as a chemical affinity or a physical constraint. The trend portrays that the increased DoS is leading to increased crosslinking density in the gels. The effect is more readily apparent at lower DoS and has less of an effect as DoS increases, although still significant. The LF NMR data agrees with the other data collected and previously discussed on these PHA gel samples.

PHA Degradation Analysis with Hyaluronidase

The enzymatic degradation rate of PHA hydrogels was assessed to investigate the impact of increased crosslinking density on the ability for the hyaluronidase to diffuse into the bulk and react with the glycosidic bond in the HA repeat unit. Degradation rate was determined via mass loss assessment in an accelerated test in which the hyaluronidase was used, 500 U/mL (10 times levels used in literature and incubated at 37°C)[46]. Figure 27 shows the rates of enzymatic degradation for all PHA DoS. The lower rate DoS PHAs, 22% and 34%, degraded rapidly. The 5 mm samples were degraded past the limits of detection, LOD, within 4 days. The LOD is the point at which the test article could not be effectively measured because the remaining degraded samples were too small to recover. For the remaining PHA samples: 47% PHA degraded to the LOD after 6 days, 70% PHA after 11 days and at the end of the 14 days test period the 90% PHA had not fully degraded. During testing, it was observed that the higher the crosslinking the less the PHAs swelled and the less color that was taken in throughout the samples incubated with

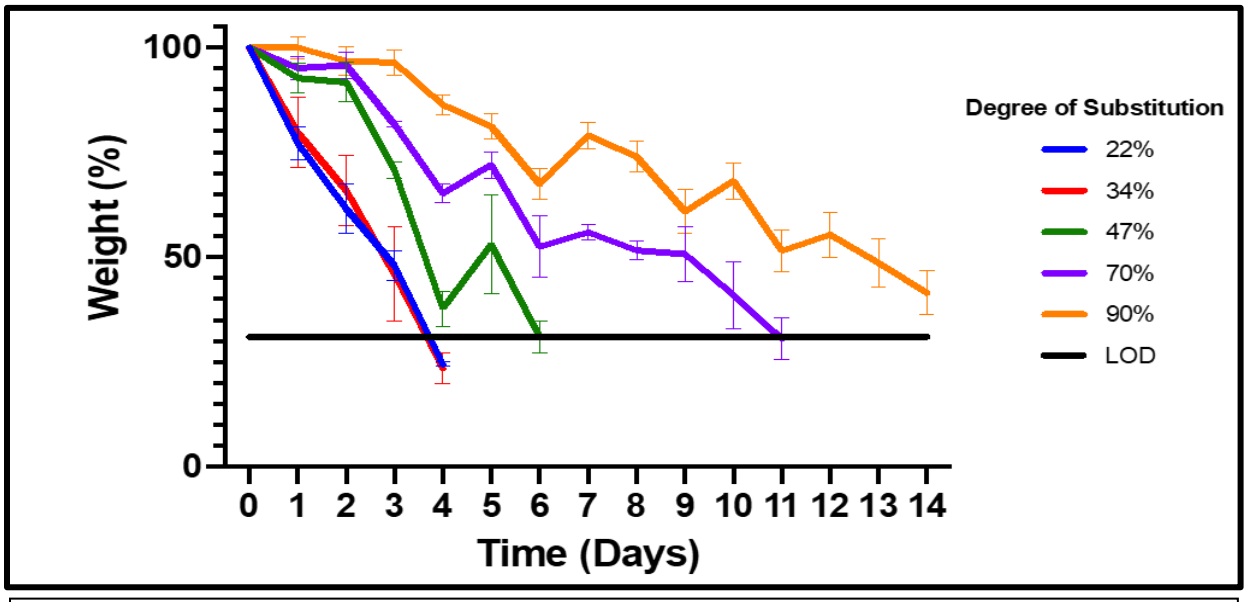

Figure 27. Enzymatic Degradation of PHA with Hyaluronidase. The line labeled LOD is the limit of detection. The blue line is 22% DoS, red is 34% DoS, green is 47% DoS, purple is 70% DoS and orange is 90% DoS.

enzyme, which added a pale, yellow tint to the solution. Figure 28 shows the rate of degradation for the control series for the accelerated degradation assay. These samples were identical to the experimental run shown in Figure 27, but there was no Hyaluronidase added to the system for these samples.

The results show that there was hydrolytic degradation at the ester of the crosslink; however, at a slower rate than the accelerated enzymatic degradation. The hydrolysis rates followed similar trends, increasing the DoS resulted in a decrease in degradation rate. The 22% and 34% showed significant degradation without the enzyme present, losing 30% and 60% of their mass, respectively. The 47% and the 70% PHAs lost ~10% of their mass and the 90% PHA showed almost

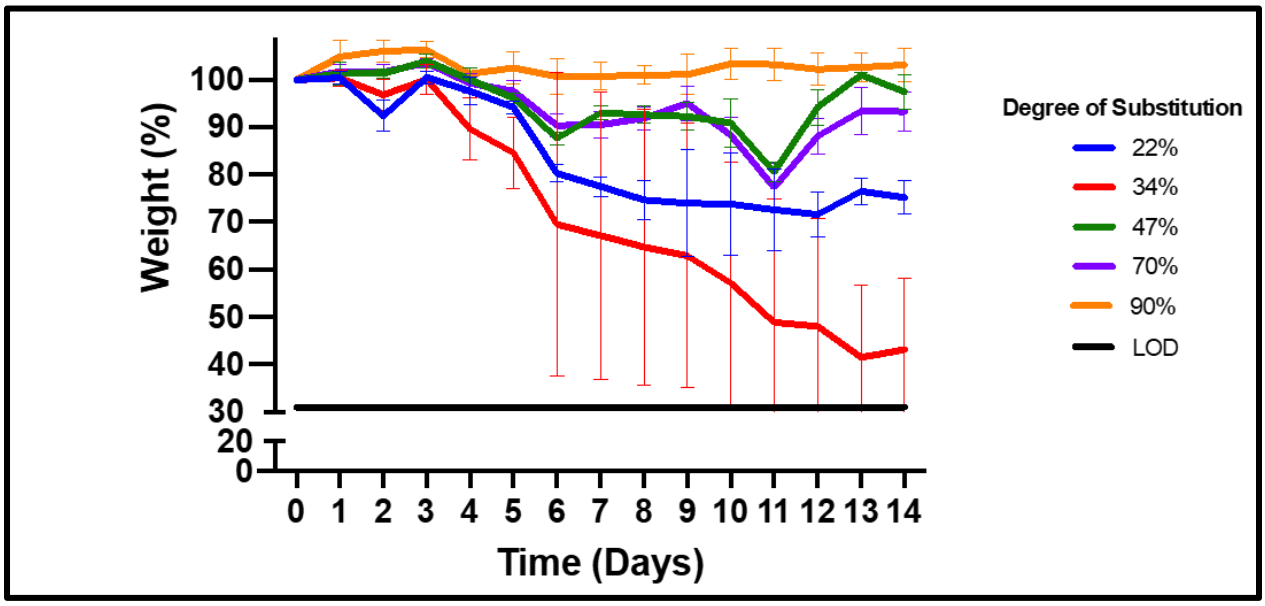

Figure 28. Degradation of PHA with no Hyaluronidase, Control assay. The line labeled LOD is the limit of detection. The blue line is 22% DoS, red is 34% DoS, green is 47% DoS, purple is 70% DoS and orange is 90% DoS.

no degradation. The samples also exhibited more edge degradation with the higher DoS samples and appeared to have an intact central core for a longer period. These results showed that with less crosslinking for the PHAs at the lower DoS the test articles were exposed to more bulk degradation. The higher the DoS the less accessible the hydrogels were to being permeated with Hyaluronidase or even swelling and taking on more water and thus limiting degradation to surface only.

The results of this assay show that even though the glycosidic bonds are being broken on the HA backbone in the PHA the pentanoate crosslinked chains are holding together. This further supports previous conclusions of increased DoS resulting in increased crosslinking as an increased number of crosslinks will limit accessibility to internal HA glycosidic bonds and result in longer degradation time.

PHA DoS Mixture

In order to determine whether the effects from DoS could be further tuned, PHA of differing DoS were combined to match the DoS of a single PHA product. In this study, PHA with a DoS of 46% was compared to a PHA mixture made using 34% and 70% DoS to make a 47% DoS sample. Figure 29 shows the comparative data for the of a 46% DoS and the 47% DoS from the created PHA mixture. Figure 30 shows the comparative data for the compressive secant modulus from DMA on the same samples.

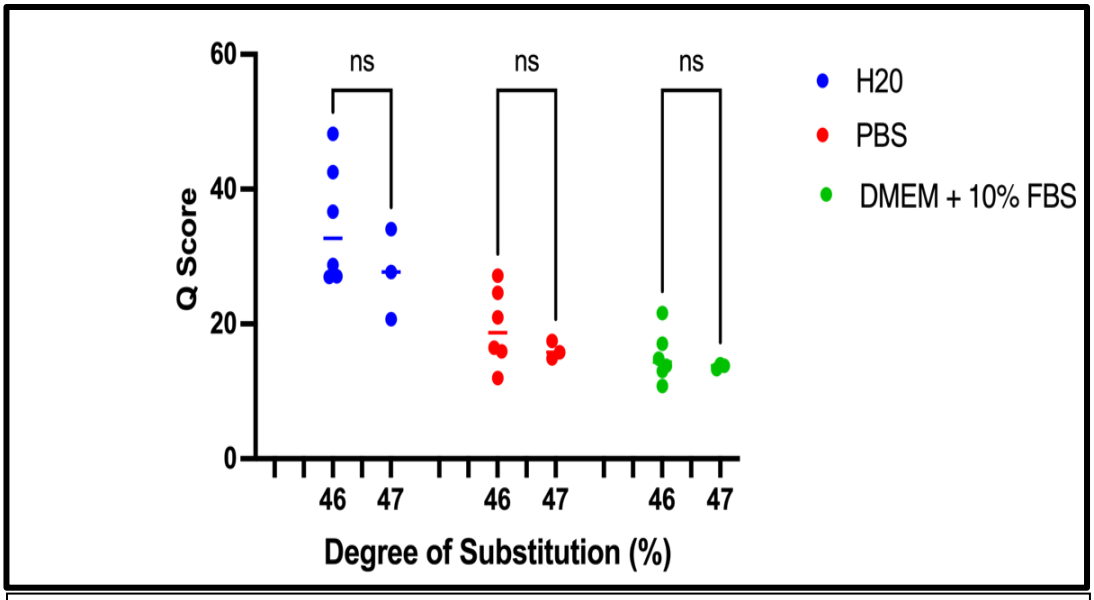

Figure 29. Swelling Scores comparing a 46% DoS chemistry versus a 47% DoS from PHA mixture in UP water, PBS and DMEM+.

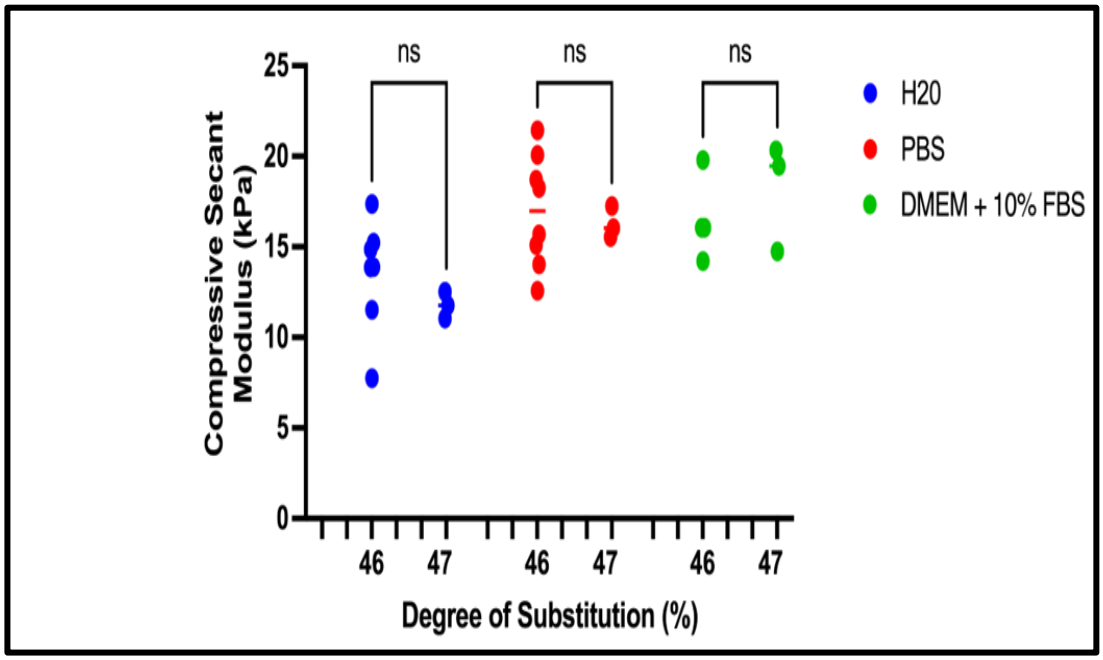

Figure 30. Compressive secant modulus of a 46% DoS chemistry versus a 47% DoS from PHA mixture in UP water, PBS and DMEM+.

No statistically significant differences were observed between the 46% gel and the 47% gel from the mixture of PHAs when compared inside the same buffer. Swelling data shows that producing PHA hydrogels from a mixture of PHAs also gives the same results. The swelling ratios in UP water, PBS and DMEM+ are statistically non-significant. It is not possible to tell the difference between the performance of hydrogels made from either method. The results are comparative to those reported in the swelling section of this paper. The PBS and DMEM+ show to have lower swelling ratios than the same samples in UP water. There are also no statistical differences observed between 46% gels and 47% gels from mixture of PHAs from compression testing. The compressive secant modulus values for all samples were almost identical. This holds for samples in UP water, PBS and DMEM+. The data shows that gels from mixture are the same gels from a direct chemical reaction. The ability to mix a PHA to any given DoS is extremely valuable. This offers the ability to create the exact DoS desired. PHA synthesis reactions take considerable time to produce. Mixtures can be made instantly from existing PHA materials.

Limitations and Future Considerations

Although the work presented in this study is robust and informative, there are some positions that should be addressed for their limitations and considerations for future work that would be beneficial to add to the value of the stated research position.

First, the work presented is looking to address needs for functionalized HA based hydrogels to be used as “mimics” of native ECM to investigate cell adhesion and differentiation in tissue engineering for meniscal regeneration. This study covered a single HA molecular weight, gels were formed at a single weight percentage, and a single wavelength and length of time for photoinitiation. It is understood that all these factors can affect studies that are designed to integrate live cells into hydrogels. Also, understood is that the molecular weight of HA can have

distinctly different effects for cellular response: pro- or anti- inflammatory, varied differentiation pathways, and different binding efficiencies for receptors like CD44. By further investigating these parameters and their effects on the physical and mechanical properties of the gel network, the system could be further optimized for use as an *in vitro* cell adhesion model.

Second, the ratio of thiol:ene used during this study was 1:1. This was effective for ensuring that hydrogels were rigid and robust for mechanical studies. The data suggest that this may also have led to complications with ene-ene reactions or intramolecular bonding of thiol-ene groups instead of intermolecular. Previous work has shown that for functionalized HA hydrogels a ratio of 0.6:1 may be more optimal[45]. Running future experiments closer to the optimal ratio may offer a wider control of the range of physical and mechanical properties for the gels.

Third, studies of the viscoelastic properties of the gels were performed using a RSA-III DMA instrument. The study was run in compression and with a uniaxial load. The calculation for storage and loss modulus were thus calculated as a position of the geometry in compression, not taking into account true shear. This may not be the most effective method to determine the true viscoelastic properties of a complex system. In the future there may be value added in performing these analyses using a rheological system.

Lastly, this study only investigated a single molecular weight of HA for production of hydrogels. Having shown that the mechanical properties of PHA mixtures were nearly identical to those of pure PHA, it would be interesting to see if mixtures of PHAs produced from different molecular weight species of HA could increase the capabilities and ranges for the physical, mechanical and cell adhesion properties of the PHA networks.

Conclusions

The ability to manufacture a hydrogel network that is capable of mimicking the physical, chemical and viscoelastic properties of the native meniscal ECM could be vital to understanding cellular proliferation, migration, differentiation needed for tissue regeneration and reduced onset of osteoarthritis. Having a hydrogel with similar viscoelastic properties to the ECM of native meniscal tissue fits well with the desire to model an *in vitro* system that would exert the same stress relaxation values to adhered cells as would be seen in native tissue. The data produced in this thesis demonstrates that the chemistry of functionalization of HA with PA is both robust and reproducible. Manipulating molar ratio of HA to PA resulted in fine control of DoS across a wide range of values. Trends showed increasing DoS resulted in increased crosslink density, reduced swelling, and increased compressive modulus. The effects of osmotic deswelling were apparent in PBS and DMEM+ where the compressive moduli were consistently lower than those in water, across all DoS. Frequency sweep studies showed storage and loss moduli at 1 Hz, in the same range as reported values for soft tissue and the ECM at the same frequency. LF-NMR illustrated a decrease in T2 relaxation times with an increase in DoS suggesting a decrease in mesh size which corroborates the swelling and compressive data. Data collected using mixtures of functionalized PHAs to generate a specific DoS hydrogel demonstrated that mixtures maintained the same properties as single batch PHA DoS. This illustrates an additional tool to tune the DoS and network formation. The PHA gels produced from mixtures of PHAs with different DoS resulted in the same swelling and mechanical observations as were seen in a single batch PHA with the same DoS. Lastly, the rate of degradation via enzymatic and hydrolytic mechanisms increased with decreasing DoS. Overall, the results from all key studies support that manipulating DoS works as a controllable tool to modulate crosslinking density and physical hydrogel properties and thus

viscoelasticity for use in *in vitro* studies to understand meniscal fibrochondrocyte mechanotransduction mechanisms.

References

1. Rey-Rico, A.; Cucchiarini, M.; Madry, H., Hydrogels for precision meniscus tissue engineering: a comprehensive review. *Connect Tissue Res* **2017,** *58* (3-4), 317-328.
2. Katz, J. N.; Arant, K. R.; Loeser, R. F., Diagnosis and Treatment of Hip and Knee Osteoarthritis: A Review. *JAMA* **2021,** *325* (6), 568-578.
3. Kloppenburg, M.; Berenbaum, F., Osteoarthritis year in review 2019: epidemiology and therapy. *Osteoarthritis Cartilage* **2020,** *28* (3), 242-248.
4. Koh, R. H.; Jin, Y.; Kim, J.; Hwang, N. S., Inflammation-Modulating Hydrogels for Osteoarthritis Cartilage Tissue Engineering. *Cells* **2020,** *9* (2).
5. Jain, K.; Ravikumar, P., Recent advances in treatments of cartilage regeneration for knee osteoarthritis. *Journal of Drug Delivery Science and Technology* **2020,** *60*.
6. Cui, A.; Li, H.; Wang, D.; Zhong, J.; Chen, Y.; Lu, H., Global, regional prevalence, incidence and risk factors of knee osteoarthritis in population-based studies. *EClinicalMedicine* **2020,** *29-30*, 100587.
7. Ondresik, M.; Azevedo Maia, F. R.; da Silva Morais, A.; Gertrudes, A. C.; Dias Bacelar, A. H.; Correia, C.; Goncalves, C.; Radhouani, H.; Amandi Sousa, R.; Oliveira, J. M.; Reis, R. L., Management of knee osteoarthritis. Current status and future trends. *Biotechnol Bioeng* **2017,** *114* (4), 717-739.
8. Rai, V.; Dilisio, M. F.; Dietz, N. E.; Agrawal, D. K., Recent strategies in cartilage repair: A systemic review of the scaffold development and tissue engineering. *J Biomed Mater Res A* **2017,** *105* (8), 2343-2354.
9. Park, Y. B.; Ha, C. W.; Lee, C. H.; Yoon, Y. C.; Park, Y. G., Cartilage Regeneration in Osteoarthritic Patients by a Composite of Allogeneic Umbilical Cord Blood-Derived Mesenchymal Stem Cells and Hyaluronate Hydrogel: Results from a Clinical Trial for Safety and Proof-of-Concept with 7 Years of Extended Follow-Up. *Stem Cells Transl Med* **2017,** *6* (2), 613-621.
10. Filardo, G.; Perdisa, F.; Roffi, A.; Marcacci, M.; Kon, E., Stem cells in articular cartilage regeneration. *J Orthop Surg Res* **2016,** *11*, 42.
11. Russu, O. M.; Pop, T. S.; Feier, A. M.; Trambitas, C.; Incze-Bartha, Z.; Borodi, P. G.; Gergely, I.; Zuh, S. G., Treatment Efficacy with a Novel Hyaluronic Acid-Based Hydrogel for Osteoarthritis of the Knee. *J Pers Med* **2021,** *11* (4).
12. Zhao, W.; Jin, X.; Cong, Y.; Liu, Y.; Fu, J., Degradable natural polymer hydrogels for articular cartilage tissue engineering. *Journal of Chemical Technology & Biotechnology* **2013,** *88* (3), 327-339.
13. Grogan, S. P.; Pauli, C.; Lotz, M. K.; D'Lima, D. D., Relevance of meniscal cell regional phenotype to tissue engineering. *Connect Tissue Res* **2017,** *58* (3-4), 259-270.
14. Chaudhuri, O.; Cooper-White, J.; Janmey, P. A.; Mooney, D. J.; Shenoy, V. B., Effects of extracellular matrix viscoelasticity on cellular behaviour. *Nature* **2020,** *584* (7822), 535-546.
15. Bochynska, A. I.; Hannink, G.; Grijpma, D. W.; Buma, P., Tissue adhesives for meniscus tear repair: an overview of current advances and prospects for future clinical solutions. *J Mater Sci Mater Med* **2016,** *27* (5), 85.
16. McNulty, A. L.; Guilak, F., Mechanobiology of the meniscus. *J Biomech* **2015,** *48* (8), 1469-78.
17. Makris, E. A.; Hadidi, P.; Athanasiou, K. A., The knee meniscus: structure-function, pathophysiology, current repair techniques, and prospects for regeneration. *Biomaterials* **2011,** *32* (30), 7411-31.
18. Shimomura, K.; Bean, A. C.; Lin, H.; Nakamura, N.; Tuan, R. S., In Vitro Repair of Meniscal Radial Tear Using Aligned Electrospun Nanofibrous Scaffold. *Tissue Eng Part A* **2015,** *21* (13-14), 2066-75.
19. Patel, H.; Skalski, M. R.; Patel, D. B.; White, E. A.; Tomasian, A.; Gross, J. S.; Vangsness, C. T.; Matcuk, G. R., Jr., Illustrative review of knee meniscal tear patterns, repair and replacement options, and imaging evaluation. *Clin Imaging* **2021,** *69*, 4-16.

20. Fisher, M. B.; Henning, E. A.; Soegaard, N.; Bostrom, M.; Esterhai, J. L.; Mauck, R. L., Engineering meniscus structure and function via multi-layered mesenchymal stem cell-seeded nanofibrous scaffolds. *J Biomech* **2015,** *48* (8), 1412-9.
21. Mohand-Kaci, F.; Assoul, N.; Martelly, I.; Allaire, E.; Zidi, M., Optimized hyaluronic acid-hydrogel design and culture conditions for preservation of mesenchymal stem cell properties. *Tissue Eng Part C Methods* **2013,** *19* (4), 288-98.
22. Necas, J., Bartosikova, L., Brauner, P., Kolar, J., Hyaluronic acid (hyaluronan): a review. *Veterinarni Medicina* **2008,** *53* (8), 14.
23. Muir, V. G.; Burdick, J. A., Chemically Modified Biopolymers for the Formation of Biomedical Hydrogels. *Chem Rev* **2021,** *121* (18), 10908-10949.
24. Lam, J.; Truong, N. F.; Segura, T., Design of cell-matrix interactions in hyaluronic acid hydrogel scaffolds. *Acta Biomater* **2014,** *10* (4), 1571-1580.
25. Means, A. K.; Grunlan, M. A., Modern Strategies To Achieve Tissue-Mimetic, Mechanically Robust Hydrogels. *ACS Macro Lett* **2019,** *8* (6), 705-713.
26. Zheng Shu, X.; Liu, Y.; Palumbo, F. S.; Luo, Y.; Prestwich, G. D., In situ crosslinkable hyaluronan hydrogels for tissue engineering. *Biomaterials* **2004,** *25* (7-8), 1339-48.
27. Snetkov, P.; Zakharova, K.; Morozkina, S.; Olekhnovich, R.; Uspenskaya, M., Hyaluronic Acid: The Influence of Molecular Weight on Structural, Physical, Physico-Chemical, and Degradable Properties of Biopolymer. *Polymers (Basel)* **2020,** *12* (8).
28. Itano, N., Simple primary structure, complex turnover regulation and multiple roles of hyaluronan. *J Biochem* **2008,** *144* (2), 131-7.
29. Bencherif, S. A.; Srinivasan, A.; Horkay, F.; Hollinger, J. O.; Matyjaszewski, K.; Washburn, N. R., Influence of the degree of methacrylation on hyaluronic acid hydrogels properties. *Biomaterials* **2008,** *29* (12), 1739-49.
30. Gloria, A.; Borzacchiello, A.; Causa, F.; Ambrosio, L., Rheological characterization of hyaluronic acid derivatives as injectable materials toward nucleus pulposus regeneration. *J Biomater Appl* **2012,** *26* (6), 745-59.
31. Bhattacharya, D.; Svechkarev, D.; Souchek, J. J.; Hill, T. K.; Taylor, M. A.; Natarajan, A.; Mohs, A. M., Impact of structurally modifying hyaluronic acid on CD44 interaction. *J Mater Chem B* **2017,** *5* (41), 8183-8192.
32. Kellett-Clarke, H.; Stegmann, M.; Barclay, A. N.; Metcalfe, C., CD44 Binding to Hyaluronic Acid Is Redox Regulated by a Labile Disulfide Bond in the Hyaluronic Acid Binding Site. *Plos One* **2015,** *10* (9).
33. Lu, P.; Takai, K.; Weaver, V. M.; Werb, Z., Extracellular matrix degradation and remodeling in development and disease. *Cold Spring Harb Perspect Biol* **2011,** *3* (12).
34. Cantini, M.; Donnelly, H.; Dalby, M. J.; Salmeron-Sanchez, M., The Plot Thickens: The Emerging Role of Matrix Viscosity in Cell Mechanotransduction. *Adv Healthc Mater* **2020,** *9* (8), e1901259.
35. Nam, S.; Lee, J.; Brownfield, D. G.; Chaudhuri, O., Viscoplasticity Enables Mechanical Remodeling of Matrix by Cells. *Biophys J* **2016,** *111* (10), 2296-2308.
36. Eddhahak, A.; Zidi, M., Influence of viscoelastic properties of an hyaluronic acid-based hydrogel on viability of mesenchymal stem cells. *Biomed Mater Eng* **2015,** *26* (3-4), 103-14.
37. Martino, F.; Perestrelo, A. R.; Vinarsky, V.; Pagliari, S.; Forte, G., Cellular Mechanotransduction: From Tension to Function. *Front Physiol* **2018,** *9*, 824.
38. Mintz, B. R.; Cooper, J. A., Jr., Hybrid hyaluronic acid hydrogel/poly(varepsilon-caprolactone) scaffold provides mechanically favorable platform for cartilage tissue engineering studies. *J Biomed Mater Res A* **2014,** *102* (9), 2918-26.
39. Hui, E.; Moretti, L.; Barker, T. H.; Caliari, S. R., The Combined Influence of Viscoelastic and Adhesive Cues on Fibroblast Spreading and Focal Adhesion Organization. *Cell Mol Bioeng* **2021,** *14* (5), 427-440.

40. Hui, E.; Gimeno, K. I.; Guan, G.; Caliari, S. R., Spatiotemporal Control of Viscoelasticity in Phototunable Hyaluronic Acid Hydrogels. *Biomacromolecules* **2019,** *20* (11), 4126-4134.
41. Galarraga, J. H.; Locke, R. C.; Witherel, C. E.; Stoeckl, B. D.; Castilho, M.; Mauck, R. L.; Malda, J.; Levato, R.; Burdick, J. A., Fabrication of MSC-laden composites of hyaluronic acid hydrogels reinforced with MEW scaffolds for cartilage repair. *Biofabrication* **2021,** *14* (1).
42. Mergy, J.; Fournier, A.; Hachet, E.; Auzély-Velty, R., Modification of polysaccharides via thiol-ene chemistry: A versatile route to functional biomaterials. *Journal of Polymer Science Part A: Polymer Chemistry* **2012,** *50* (19), 4019-4028.
43. Townsend, J. M.; Andrews, B. T.; Feng, Y.; Wang, J.; Nudo, R. J.; Van Kampen, E.; Gehrke, S. H.; Berkland, C. J.; Detamore, M. S., Superior calvarial bone regeneration using pentenoate-functionalized hyaluronic acid hydrogels with devitalized tendon particles. *Acta Biomater* **2018,** *71*, 148-155.
44. Kiyotake, E. A.; Douglas, A. W.; Thomas, E. E.; Nimmo, S. L.; Detamore, M. S., Development and quantitative characterization of the precursor rheology of hyaluronic acid hydrogels for bioprinting. *Acta Biomater* **2019,** *95*, 176-187.
45. Van Kampen, E. Controlling Protein Permeability in Hydrogels for Drug Delivery Applications. The University of Kansas, ProQuest, 2016.
46. Lee, H. Y.; Hwang, C. H.; Kim, H. E.; Jeong, S. H., Enhancement of bio-stability and mechanical properties of hyaluronic acid hydrogels by tannic acid treatment. *Carbohydr Polym* **2018,** *186*, 290-298.
47. Horkay, F.; Magda, J.; Alcoutlabi, M.; Atzet, S.; Zarembinski, T., Structural, mechanical and osmotic properties of injectable hyaluronan-based composite hydrogels. *Polymer (Guildf)* **2010,** *51* (19), 4424-4430.
48. Tomer, R., Dimitrijevic, D., Florence, A., Electrically controlled release of macromolecules from cross-linked hyaluronic acid hydrogels *Journal of Controlled Release* **1995,** *33*, 8.
49. Li, Q.; Qu, F.; Han, B.; Wang, C.; Li, H.; Mauck, R. L.; Han, L., Micromechanical anisotropy and heterogeneity of the meniscus extracellular matrix. *Acta Biomater* **2017,** *54*, 356-366.